Master thesis

Reanalysis of CMS Dilepton + Dijet data from the LHC in LR extensions of the Standard Model

Daniel Schwartländer
Matrikelnummer: 363646

Supervisor and first examiner: Prof. Dr. Michael Klasen
Second examiner: Jun. Prof. Dr. Anna Kulesza

30.10.2015

Contents

Chapter 1

Introduction

The Standard Model of particle physics (SM) is a very successful theory, which describes three of the four known fundamental forces with a high precision. After the discovery of the Higgs boson (or a particle consistent with its properties) at the Large Hadron Collider (LHC) [1, 2] the last particle that was predicted by the SM is found. Yet there is still a number of unsolved issues within the Standard Model as well as experimental observations that can not be explained by the SM. This leaded to the proposal of many different theories beyond the SM (BSM) with new interactions and particles. The search for such new physics is one of the main purposes of the LHC. Since all BSM models have to incorporate the SM as a low energy effective theory, all BSM processes are very likely suppressed. Thus, BSM events are expected to be rare even at the energy of the LHC and looking for them in the huge number of total events can be very difficult.

One class of well-motivated BSM models are the left-right symmetric extensions of the SM. They could lead to rather distinctive signals at the LHC.

A strange aspect of the SM is the maximal parity violation by weak interactions. While electromagnetic and strong interactions preserve parity, the Z and W bosons couple only to left-handed fermions. Left-right symmetric models (LR models) were originally introduced to explain the parity violation and to restore parity at high scales [3, 4, 5, 6, 7]. In LR models an additional $SU(2)_R$ is spontaneously broken at a scale that is much higher than the electroweak symmetry breaking scale. The spontaneous symmetry breaking introduces three new massive gauge bosons Z_R and $W_R^{\pm}$ additionally to the three massive gauge bosons of the SM.

Another issue of the SM is the experimental observation of neutrino oscillations, which implies nonzero neutrino masses. Since the neutrino masses are much smaller than the masses of other fermions, the question of the origin of neutrino masses arises. It was found that it is possible to connect the generation of very light neutrino masses with the parity violation in LR models via the seesaw mechanism [8]. Additionally to three light neutrinos the seesaw mechanism also gives rise to three heavy Majorana neutrinos.

Their existence together with the additional right-handed gauge bosons leads to the Keung-

Senjanovič process, which could be detected at the LHC. This signal was already studied by the CMS collaboration in [9, 10] to set limits on the mass of the W_R and the mass of the heavy Majorana neutrinos.

The aim of this work is to reproduce the CMS results with a different set of public simulation tools for collider physics. Particularly, the detector simulation of CMS is replaced by a simpler but also much faster simulation. Once a validated version of the analysis exists, it is possible to use it for different variants of the LR-model and to combine it with other searches and constraints from high precision data.

Chapter 2

Theory

This chapter provides a short overview of the physics, relevant definitions and models.

1 Kinematics at the LHC

The commonly used variables to describe the collision of two particles at high velocities are outlined in this section. A more detailed description of the variables and the conventions can be found in [11, 12].

CMS uses a coordinate system where the origin is located at the collision point. The z-axis is in the same direction as the beam, while the y-axis is pointing upwards. The x-axis points to the centre of the LHC [12]. All the physics is then described relative to the beam axis (z-axis).

Instead of the polar angle θ in a spherical coordinate system one uses the pseudorapidity

$$\eta = -\ln\left(\tan\left(\frac{\theta}{2}\right)\right), \tag{2.1}$$

which originates from relativistic kinematics. To switch from the lab frame to a frame of a moving particle in the beam one has to use a Lorentz boost in the z-direction. One possible representation of this boost is

$$\begin{pmatrix} t' \\ z' \end{pmatrix} = \begin{pmatrix} \cosh(y) & \sinh(y) \\ \sinh(y) & \cosh(y) \end{pmatrix} \begin{pmatrix} t \\ z \end{pmatrix} \tag{2.2}$$

with the rapidity y. A comparison with the standard Lorentz transformation gives

$$\cosh(y) = \frac{1}{\sqrt{1-v^2}} \tag{2.3}$$

$$\sinh(y) = v_z \frac{1}{\sqrt{1-v^2}} \tag{2.4}$$

with the velocity in z-direction v_z. This leads to

$$E = m\cosh(y) \tag{2.5}$$
$$p_z = m\sinh(y) \tag{2.6}$$

and

$$y = \operatorname{arctanh}\left(\frac{p_z}{E}\right) = \frac{1}{2}\ln\left(\frac{E+p_z}{E-p_z}\right). \tag{2.7}$$

For high velocities the approximation $E \approx p$ gives the pseudorapidity

$$y \approx \frac{1}{2}\ln\left(\frac{p+p_z}{p-p_z}\right) = \frac{1}{2}\ln\left(\frac{1+\cos(\theta)}{1-\cos(\theta)}\right) = -\ln\left(\tan\left(\frac{\theta}{2}\right)\right) = \eta. \tag{2.8}$$

The pseudorapidity can also be used to define a cone around a particle direction or a measure of angular separation of two particles, that is invariant under boosts in the z-direction

$$\Delta R = \sqrt{(\Delta\eta)^2 + (\Delta\phi)^2} \tag{2.9}$$

where $\Delta a = a_1 - a_2$ is just a difference and ϕ is the azimuthal angle. Additional used variables are the transverse momentum

$$p_{\mathrm{T}} = \sqrt{p_x^2 + p_y^2} \tag{2.10}$$

and the i-object mass distribution

$$M_{\mathrm{particle}_1,\mathrm{particle}_2,\ldots,\mathrm{particle}_i} = \sqrt{(\sum_i p_{\mathrm{particle}_i})_\mu (\sum_i p_{\mathrm{particle}_i})^\mu}. \tag{2.11}$$

2 Drell-Yan Process

The Drell-Yan process is the production of two leptons l^+l^- and some additional final state particles X through a collision of two hadrons H_A and H_B like two protons or one proton and one anti-proton with momenta p_1 and p_2

$$H_A(p_1) + H_B(p_2) \to l^+ + l^- + X. \tag{2.12}$$

It is the prototype for the calculation of cross sections for hadron colliders like the LHC.

Protons are bound states consisting of quarks and gluons (the so called partons), which interact via Quantum Chromodynamics (QCD). The coupling constant g_S of QCD depends on the renormalization scale μ. With the help of the renormalization group equations one gets the equation [13]

$$\alpha_S(\mu^2) = \frac{4\pi}{(11 - \frac{2}{3}N_f)\ln\left(\frac{\mu^2}{\Lambda^2}\right)} \tag{2.13}$$

for the scale dependence of the running fine-structure constant $\alpha_S = \frac{g_S}{4\pi}$, where Λ is the strong interaction scale and N_f is the number of effective massless quark flavours. Since the denominator is positive, it is possible to divide the behaviour of QCD in the following two regions. Energy scales smaller than Λ result in large α_S. This is the region of confinement, which leads to the hadronization of coloured particles and can not be treated perturbatively. $\mu > \Lambda$ decreases α_S, which goes to zero for asymptotically large scales $\mu \to \infty$. This property is called asymptotic freedom and it is therefore tempting to set μ equal to the energy or momentum scale of the process Q and to use perturbation theory for the computation of cross sections at high energies. Nevertheless it turns out that the long distance physics of the proton can not be neglected in the hadron hadron collisions.

The hadronic cross section $\sigma_{H_1H_2 \to l^+l^- + X}$ can still be calculated by perturbation with the help of the QCD factorization theorem [14]. It separates the process into the hard scattering of the partons and a soft part, which is included by the parton distribution functions (PDFs) $f_i^A(x_1)$. The PDF $f_i^A(x_1)$ gives the number density (in the infinite momentum frame) of parton i in hadron A. It depends on the fraction $x_1 \in [0, 1]$ that the parton carries of the momentum of hadron A. Since it can not be calculated from theory, it is taken from experiments. In the hard process partons i of hadron A and partons j of hadron B scatter with the partonic cross section σ_{ij}, where each parton carries the momentum $p_{1(2)} = x_{1(2)}p_{1(2)}$. The differential hadronic cross section is then given by the convolution of the partonic cross section and the parton distribution functions:

$$\mathrm{d}\sigma_{H_1H_2 \to l^+l^- + X} = \sum_{i,j} \int_0^1 \mathrm{d}x_1 \mathrm{d}x_2 f_i^A(x_1) f_j^B(x_2) \mathrm{d}\sigma_{ij}. \tag{2.14}$$

$\mathrm{d}\sigma_{ij}$ is the differential partonic cross section, which is at leading order

$$\mathrm{d}\sigma_{ij} = \frac{1}{2s} |\overline{M}|^2 \mathrm{d}PS^{(2)}, \tag{2.15}$$

where $\mathrm{d}PS^{(2)}$ is the phase space of the two final state particles, $\frac{1}{2s}$ the flux factor and $|\overline{M}|^2$ is the squared averaged invariant matrix element, which is calculated perturbatively.

3 Event generators

This section gives a short overview of event generators, which are used to simulate the final state of high energy collision at an accelerator like the LHC. It follows the description of [11] and [15]. More detailed information to event generators and the underlying physics can be found in the manuals of different event generators such as [15, 16, 17].

3.1 Hard scattering

The simulation of a process starts with the calculation of the hadronic cross section. In order to do this the generator requires the matrix elements of the partonic cross section.

This matrix elements are implemented by the user, are already provided by the generator or are generated by the event generator itself. They are usually calculated at the leading order or at next to leading order. Then the hadronic cross section is computed from the convolution of the differential partonic cross section with the PDFs and the integration over the phase space. The integration is done with a Monte Carlo method, which at the same time gives the momentum distributions for the simulated events from the sampling.

3.2 Parton shower

All coloured final and initial state particles of the hard scattering process can emit gluons, which leads to a rapidly increased number of final state particles (a "shower" of hadronic particles). It is therefore necessary to include this large number of particles in the simulation to get a more realistic event. The first approach would be to calculate the hard scattering process to higher orders in perturbation theory, which becomes much more difficult for every order. A second possibility is the parton shower, which approximates the probability that a branching $a \to b\ c$ like $q \to q\ g$ or $g \to g\ g$ takes place. The produced particles themselves can then also emit. This procedure has the advantage that there is no upper limit on the number of the final state particles (like in fixed order calculations) and that it is simpler than the former approach.

The parton shower approach is motivated by the large corrections that exclusive observables receive from collinear and infrared singularities. A collinear splitting is of order $\alpha_S(Q) \ln\left(\frac{Q}{\Lambda}\right)$, if a infrared cut-off defined by the hadronization scale is used. Because of $\alpha_S \sim \frac{1}{\ln\left(\frac{Q}{\Lambda}\right)}$ (see eq. 2.13) it leads to corrections of order unity. Therefore the dominant region of phase space is a region in which all branchings can be ordered by a virtuality measure. This virtuality measure typically involves the angle and the energy of the radiation, but it is not unique and there are different choices in use. One simple choice used in final state showers is the virtuality $q^2 = E^2 - |\vec{p}|^2$ since a branching $a \to cd$ can not take place if all particles are on-shell. Each parton is then characterized by its virtuality scale, which gives an approximate time ordering. For a final state with many partons, pairs of partons can be clustered together recursively by their virtuality measure to get a branching tree.

This procedure is also the foundation of the reconstruction of jets with sequential recombination algorithms.

Another property of the dominant region in phase space are the large distances and times between following branchings. The distances and times increase with every splitting and suppress interference effects, which is also a motivation to approximate the process by a composition of probabilities instead of using the whole amplitudes.

Every branching, depending on the definition, decreases or increases the virtuality scale and if the virtuality scale of the partons exceeds the hadronization scale, the shower evolution is stopped and the hadronization is simulated.

3.3 Hadronization

The stop of the parton showering and the beginning of the hadronization marks the transition from short distance physics occurring at a time scale $\sim \frac{1}{\Lambda}$ to long distance physics, which can not be treated perturbatively. Hadronization (also called fragmentation) is the transformation of the partons into a set of colour singlets, which takes place in the region of confinement. Since there is no calculation from first principles available, there are different QCD inspired phenomenological models in use.

One class of hadronization models are the string fragmentation models or string models like the Lund model [15]. They are based on the observation in lattice QCD that the potential between a colour singlet quark anti-quark pair seems to behave like $V(r) \sim a\frac{1}{r} + br$. For large distances r the energy stored in the potential increases linearly with the separation of the quarks, which is known as linear confinement. When the Coulomb like part of the potential is neglected, the potential describes a string with a certain tension b. If the quark and anti-quark move apart, it is envisioned that a colour flux tube is stretched between the quarks. This colour flux tube is described by the dynamics of a massless relativistic string. When the energy of the string increases, the string can break by producing a new quark anti-quark pair, such that the system splits into two quark anti-quark pairs. The process can be repeated for each of the pieces, providing that the invariant mass of the piece is large enough. A singlet quark gluon anti-quark system is represented by a string that is stretched from the quark over the gluon to the anti-quark, so that a gluon is a transversal kink in the string. The kink carries energy and momentum, which makes the formerly one dimensional object two dimensional.

With this principles all colour connected partons are linked via strings and then the string fragmentations are simulated. The information concerning which subsystems of the final state are colour connected after the parton shower is transferred from the parton shower algorithm. It is determined in the large colour limit, where any branching of partons can be represented as a sum of distinct colour flows. The colour information of a quark can be depicted as a colour line with the arrow in the direction of the fermion flow. A gluon is represented as two lines with arrows in opposite direction. Figure 2.1 shows the rules for the colour flows and a simple example for showering a $q\ \bar{q}$ pair and producing three colour connected pairs is given in figure 2.2.

Overall, the string fragmentations happen until only on-shell hadrons remain, which are represented as strings connecting quark anti-quark pairs. The next step is the decay of all unstable hadrons produced by the fragmentation, where experimental data is used for the decay, if it is available.

4 $SU(2)$ conventions

There are some conventions concerning the representations of objects, that transform as doublets or triplets under one or two different $SU(2)$ gauge groups, which are shown here. This section follows mainly [18, 19], where a more detailed explanation can be found.

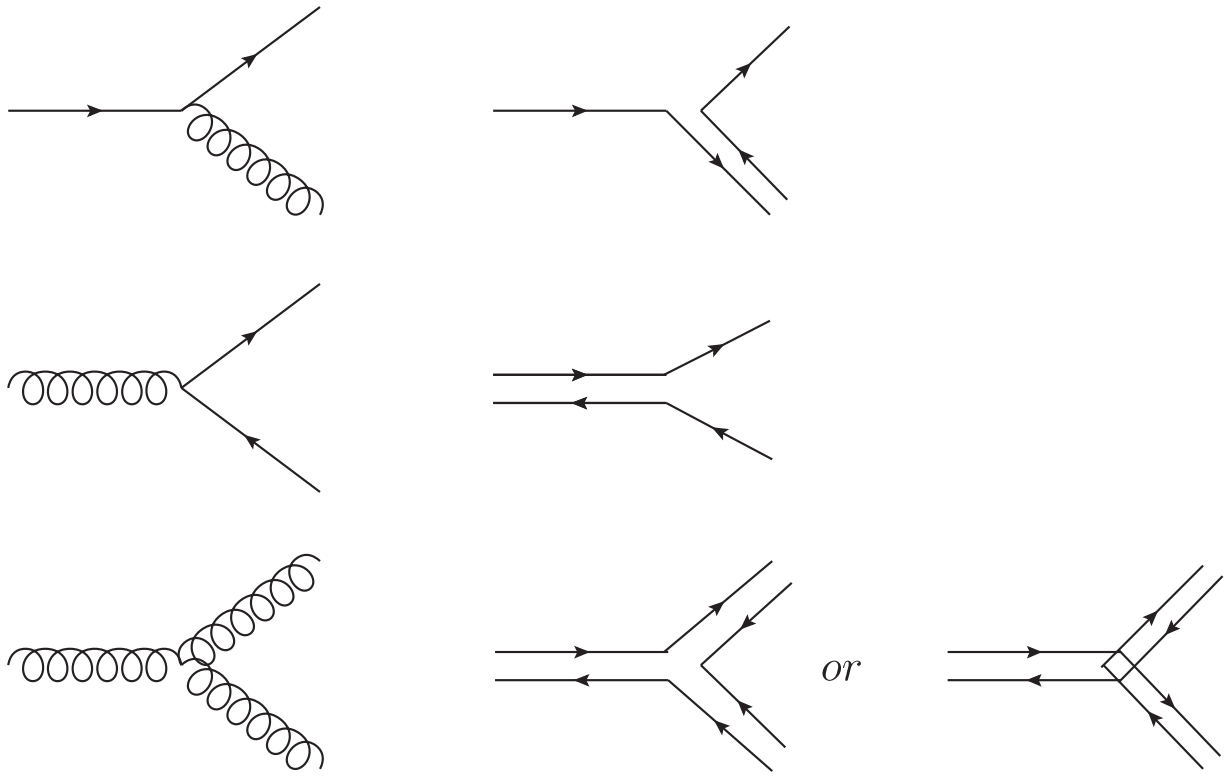

Figure 2.1: Rules for the colour flows in the large colour limit

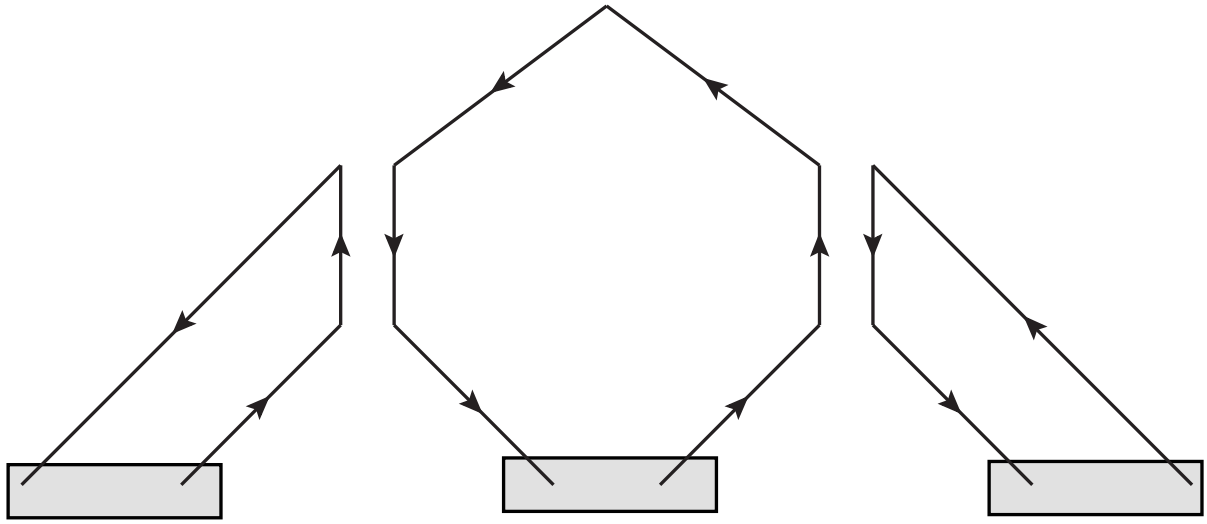

Figure 2.2: Simple example for the colour flow: a $q\ \bar{q}$ pair, which was produced in a hard scattering process, gives three pairs after the parton shower

The fundamental (two dimensional) irreducible representation, denoted as (2), can be realized by 2x2 matrices U_{ab}. Their generators T_i, that span this representation, are conventional taken to be $\frac{1}{2}\sigma_i$ by choice of phase, where σ_i are the three Pauli matrices. A two component spinor ψ then transforms as

$$\psi_a^{'} = U_a{}^b \psi_b \tag{2.16}$$

under the group action (contracting upper and lower indices).

Another representation of a Lie group is the conjugate representation $\bar{U}$ denoted here as $(\bar{2})$ with the generators $-T^*$. We use upper indices for spinors ψ^a, that transform under this representation.

It turns out that these two representations are equivalent because all Pauli matrices obey the relation

$$C\sigma_i C^{-1} = -\sigma^* \tag{2.17}$$

with the matrix

$$C = i\sigma_2 = \begin{pmatrix} 0 & 1 \\ -1 & 0 \end{pmatrix}. \tag{2.18}$$

Equation 2.17 leads to

$$CUC^{-1} = \bar{U}, \tag{2.19}$$

from which one can show, that C can be used to raise and lower indices

$$\psi^a = C^{ab}\psi_b \tag{2.20}$$

$$\psi_a = (C^{-1})_{ab}\psi^b \tag{2.21}$$

and therefore to switch between the two representations. Instead of C and C^{-1} one summarizes them and uses the total antisymmetric tensor ϵ because of the properties $\epsilon_{12} = -\epsilon_{21} = -\epsilon^{12} = \epsilon^{21} = 1$ (see 2.18).

Fields, that are doublets under two different $SU(2)$ groups (bidoublets) appear in G(221) models. Usually they are chosen to transform in the fundamental representation under the first $SU(2)$ and in the conjugate representation under the second $SU(2)$. This is denoted as $(2, \bar{2})$ and written as

$$\Psi^i{}_{\tilde{i}} = \begin{pmatrix} h_1 & h_2 \\ h_3 & h_4 \end{pmatrix}, \tag{2.22}$$

where i is the index of the first $SU(2)$ and $\tilde{i}$ is the index of the second $SU(2)$.

Another notation that is often used in literature, is the matrix representation Ψ of $SU(2)$ triplets δ [19]:

$$\Psi = \frac{1}{\sqrt{2}}\sigma_m^{'}\delta^m, \tag{2.23}$$

model	$SU(2)_1$	$SU(2)_2$
LR	$\begin{pmatrix}\nu_L\\e_L\end{pmatrix}$ $\begin{pmatrix}u_L\\d_L\end{pmatrix}$	$\begin{pmatrix}\nu_R\\e_R\end{pmatrix}$ $\begin{pmatrix}u_R\\d_R\end{pmatrix}$
LP	$\begin{pmatrix}\nu_L\\e_L\end{pmatrix}$ $\begin{pmatrix}u_L\\d_L\end{pmatrix}$	$\begin{pmatrix}u_R\\d_R\end{pmatrix}$
HP	$\begin{pmatrix}\nu_L\\e_L\end{pmatrix}$ $\begin{pmatrix}u_L\\d_L\end{pmatrix}$	$\begin{pmatrix}\nu_R\\e_R\end{pmatrix}$
FP	$\begin{pmatrix}\nu_L\\e_L\end{pmatrix}$ $\begin{pmatrix}u_L\\d_L\end{pmatrix}$	

Table 2.1: Representations of fermions for different models belonging to the first breaking pattern (LR, LP, HP and FP models) [20]

where $m = 1, 0, -1$ is the third component of the isospin and

$$\sigma_1^{'} = \frac{1}{2}(\sigma_1 + \mathrm{i}\sigma_2) \tag{2.24}$$

$$\sigma_0^{'} = \sigma_3 \tag{2.25}$$

$$\sigma_{-1}^{'} = \frac{1}{2}(\sigma_1 - \mathrm{i}\sigma_2). \tag{2.26}$$

5 G(221) models

This section mainly follows the classification and the description of [20], where a more detailed discussion can be found.

The G(221) models are a class of models that are all based on the gauge structure

$$SU(2)_1 \otimes SU(2)_2 \otimes U(1)_X. \tag{2.27}$$

This gauge structure can be seen as a low-energy effective field theory of many BSM models. It naturally occurs in some breaking patterns of gauge unification scenarios like $SO(10)$ or E_6 and extra dimensional models [19, 21]. Examples for models that use this structure are the left-right (LR), the leptophobic (LP), the hadrophobic(HP), the fermiophobic (FP), the ununified (UU) and the nonuniversal (NU) models.

These models are spontaneously broken to the SM gauge structure by one of the two different breaking patterns described below, which give rise to three new massive gauge bosons called $Z^{'}$ and $W^{'\pm}$.

In the first breaking pattern one $SU(2)$ gauge group is identified with the $SU(2)_L$ of the SM. The second $SU(2)$ is then involved in the first stage of symmetry breaking $SU(2) \otimes U(1)_X \rightarrow U(1)_Y$. Then the second stage is $SU(2)_L \otimes U(1)_Y \rightarrow U(1)_{em}$ like in the SM. LR, LP, HP and FP models all belong to this breaking pattern, but leptons and quarks transform different under the $SU(2)_2$. An overview of the representations in the different model is shown in tabular 2.1.

model	$SU(2)_1$	$SU(2)_2$
UU	$\begin{pmatrix} u_L \\ d_L \end{pmatrix}$	$\begin{pmatrix} \nu_L \\ e_L \end{pmatrix}$
NU	1st and 2nd generation: $\begin{pmatrix} \nu_L \\ e_L \end{pmatrix}$ $\begin{pmatrix} u_L \\ d_L \end{pmatrix}$	3rd generation: $\begin{pmatrix} \nu_L \\ e_L \end{pmatrix}$ $\begin{pmatrix} u_L \\ d_L \end{pmatrix}$

Table 2.2: Representations of fermions for different models belonging to the second breaking pattern (UU and NU models) [20]

For the LR models all left-handed quarks and leptons are doublets in the $SU(2)_L$ and singlets in the $SU(2)_R$, while the representations for the right-handed quarks and leptons are vice versa.

LP (HP) models are similar to the LR models, but only right-handed quarks (leptons) are $SU(2)_1$ doublets, while the right-handed leptons (quarks) are $SU(2)_1$ singlets. They can be seen as an in-between of LR and FP models, because the right-handed fermions are all $SU(2)_1$ singlets in a FP model. The LP, HP and FP models are not free of gauge anomalies and therefore their particle content is incomplete without introducing additional particles [20].

The UU and NU models have a different breaking pattern, where $U(1)_X$ is identified with $U(1)_Y$. Then $SU(2)_1 \otimes SU(2)_2 \to SU(2)_L$ is the first step of the symmetry breaking and $SU(2)_L \otimes U(1)_Y \to U(1)_{em}$ is the second. In UU models left-handed quarks transform as doublets under $SU(2)_1$ but as singlets under the $SU(2)_2$ and vice versa for left-handed leptons. The representations in NU models however depend on the generation of the fermions. Leptons and quarks of the first and second generation are $SU(2)_1$ doublets, while third generation leptons and quarks transform as $SU(2)_2$ doublets. All representations are summarized in table 2.2.

UU models also contain gauge anomalies [20], but additional particles to fix them are not considered here.

After fixing the representations of the fermions all models still contain the freedom to realize both breaking patterns with different Higgs representations. The number of Higgs particles is also not fixed. Sometimes more Higgs particles are introduced than needed for the spontaneous symmetry breaking. They are used to preserve a discrete symmetry (typically LR models) or to generate masses for all fermions (typically second breaking pattern).

5.1 LR models

The next section describes the later analysed LR model in more detail and gives some relevant formulas. The parametrization, formulas and Lagrangians developed in [20] are used, if not otherwise stated.

The previous introduced Z', $W'^{\pm}$, $SU(2)_1$ and $SU(2)_2$ are called Z_R, $W_R^{\pm}$, $SU(2)_L$ and

$SU(2)_R$ in the context of LR models. Then the LR models are based on the gauge structure

$$SU(2)_L \otimes SU(2)_R \otimes U(1)_X \tag{2.28}$$

with the coupling constants g_L, g_R and g_X. This gauge structure was introduced historically in the 70s to restore Parity conservation at high energies [3, 4, 5, 6, 7], which is possible when $g_L = g_R$ holds at a certain scale. Another attractive feature is the generation of neutrino masses, which arises naturally, because right-handed neutrinos have to be included to complete the right-handed lepton doublets [3, 4, 5, 6, 7]. Additionally there exists the possibility to handle the strong CP problem in supersymmetric LR models [22, 23, 24]. They are also free of gauge anomalies without the introduction of additional particles [20].

There exist two different conventions for the charge X assignments of the fermions. In the first convention the electric charge is given by

$$Q = T_3^{SU(2)_L} + T_3^{SU(2)_R} + X \tag{2.29}$$

and in the second by

$$Q = T_3^{SU(2)_L} + T_3^{SU(2)_R} + \frac{X}{2}, \tag{2.30}$$

where $T_3^{SU(2)_{L/R}}$ is the third component of the isospin of $SU(2)_{L/R}$ and X is the charge of $U(1)_X$. These are just modifications of the two different conventions of the SM weak hypercharge Y

$$Q = T_3 + Y \tag{2.31}$$

and

$$Q = T_3 + \frac{Y}{2}. \tag{2.32}$$

An interesting feature is the possibility to relate the charge X with the difference of the Baryon number B and the lepton number L, which gives

$$X = \frac{B - L}{2} \tag{2.33}$$

for the first convention and

$$X = B - L \tag{2.34}$$

for the second convention. This is used in the context of LR supersymmetric models to preserve and motivate R-parity [19]. We will use the first convention in the following sections.

As mentioned before, the Higgs representation is not fixed by the model and one has to choose a representation.

Higgs doublets are the minimal solution for the first stage of symmetry breaking and historically, they were the first ones considered [3, 4, 5, 6, 7].

stage	$SU(2)_L \otimes SU(2)_R \otimes U(1)_X$	Higgs multiplet	VEV
1.	$(1, 2, \frac{1}{2})$	$\Phi = \begin{pmatrix} \Phi^+ \\ \Phi^0 \end{pmatrix}$	$\langle\Phi\rangle = \frac{1}{\sqrt{2}} \begin{pmatrix} 0 \\ u_D \end{pmatrix}$
2.	$(2, \bar{2}, 0)$	$H = \begin{pmatrix} h_1^0 & h_1^+ \\ h_2^- & h_2^0 \end{pmatrix}$	$\langle H\rangle = \frac{v}{\sqrt{2}} \begin{pmatrix} \cos\beta & 0 \\ 0 & \sin\beta \end{pmatrix}$

Table 2.3: Higgs representations and vacuum expectation values for the LR model with doublets in the first breaking stage [20]

stage	$SU(2)_L \otimes SU(2)_R \otimes U(1)_X$	Higgs multiplet	VEV
1.	$(1, 3, 1)$	$\Phi = \frac{1}{\sqrt{2}} \begin{pmatrix} \Phi^+ & \sqrt{2}\Phi^{++} \\ \sqrt{2}\Phi^0 & -\Phi^+ \end{pmatrix}$	$\langle\Phi\rangle = \frac{1}{\sqrt{2}} \begin{pmatrix} 0 & 0 \\ u_T & 0 \end{pmatrix}$
2.	$(2, \bar{2}, 0)$	$H = \begin{pmatrix} h_1^0 & h_1^+ \\ h_2^- & h_2^0 \end{pmatrix}$	$\langle H\rangle = \frac{v}{\sqrt{2}} \begin{pmatrix} \cos\beta & 0 \\ 0 & \sin\beta \end{pmatrix}$

Table 2.4: Higgs representations and vacuum expectation values for the LR model with triplets in the first breaking stage [20]

The most common choice is nevertheless a Higgs triplet for the first stage of the spontaneous symmetry breaking, which can introduce a seesaw mechanism by generating Dirac and Majorana mass terms for right-handed neutrinos [8, 25]. This can explain the smallness of neutrino masses and also leads to additional heavy Majorana neutrinos with right-handed couplings [8, 25]. Although this is difficult to achieve and needs fine tuning for a TeV breaking scale [26]. Doubly charged Higgs bosons, which were the subject of many studies [27, 28, 29], arise also from Higgs triplets. The Higgs triplet approach is used here, because the following analysis assumes the existence of a heavy neutrino with right-handed couplings and it is not possible to have Majorana neutrinos in doublet models [26].

The second stage of symmetry breaking is realized by Higgs bidoublets in both cases. Many LR models have more Higgs bosons than required for spontaneous symmetry breaking like additional Higgs triplets under $SU(2)_L$ to preserve a discrete symmetry like generalized parity or charge conjugation at higher scales [19, 26]. The Higgs representations and vacuum expectation values (VEVs) for doublet and triplet models are summarized in tabular 2.3 and tabular 2.4.

The first breaking stage should take place at the TeV scale, because of existing bounds on the Z_R and W_R mass [9, 20, 30], while the second stage takes place at the electroweak scale. This plays also a role in the generation of the neutrino masses by the seesaw mechanism. If no additional Higgs bosons or symmetries are introduced, the general Yukawa interactions of the Lagrangian look like

$$\mathcal{L}_{\text{Yuk}} = y_{q1}\bar{Q}_R H Q_L + y_{q2}\bar{Q}_R \sigma_2 H^* \sigma_2 Q_L + y_{l1}\bar{l}_R H l_L + y_{l2}\bar{l}_R \sigma_2 H^* \sigma_2 l_L + y_{l3} l_R^c \mathrm{i}\sigma_2 \Phi l_R + \text{h.c.} \tag{2.35}$$

with the Yukawa couplings y_{q1}, y_{q2}, y_{l1}, y_{l2} and y_{l3}. The four Higgs bidoublet terms lead to Dirac masses for quarks and leptons, while the triplet leads to a Majorana mass term for

right-handed neutrinos. After symmetry breaking the mass Lagrangian for neutrinos is

$$\mathcal{L}_{\text{Neutrinos}} = \frac{1}{2}\left[\begin{pmatrix}\nu_L^c & \bar{\nu}_R\end{pmatrix}\begin{pmatrix}0 & m_D\\ m_D^T & m_R\end{pmatrix}\begin{pmatrix}\nu_L\\ \nu_R^c\end{pmatrix}\right], \tag{2.36}$$

where m_D is proportional to v and m_R is proportional to u_T. Since $v \ll u_T$, the first mass eigenstate N has the mass $m_N \approx m_R$ and the second eigenstate ν has $m_\nu \approx \frac{m_D^2}{m_N}$ (for one family of neutrinos or when the mixing between the families is neglected). The gauge eigenstates can be expressed by the mass eigenstates via a unitary transformation, which leads to equations of the form $\nu_L \approx \mathcal{O}(1)\nu + \mathcal{O}(\frac{m_D^2}{m_N^2})N$ and $\nu_R \approx \mathcal{O}(1)N + \mathcal{O}(\frac{m_D^2}{m_N^2})\nu$. Thus, the mixing effects of the unitary transformation can be neglected and the model contains very light Majorana neutrinos that only interact via the left-handed gauge bosons and heavy right-handed Majorana neutrinos. The mass M_{N_l} of the heavy Majorana neutrinos N_l with the flavour l is taken as a free parameter, since the Yukawa couplings are free parameters.

Now following are the formulas and definitions that are relevant for the interactions between gauge bosons and fermions. The Higgs sector itself is no longer considered here, since it is neglected in the later analysis.

After the first breaking stage arises

$$g_Y = \left(\frac{1}{g_R^2} + \frac{1}{g_X^2}\right)^{-\frac{1}{2}}, \tag{2.37}$$

which is the coupling of the $U(1)_Y$. The mixing angle ϕ of the first breaking stage is defined as

$$\tan(\phi) = \frac{g_X}{g_R}. \tag{2.38}$$

It is then convenient to introduce the mixing angle θ of the second breaking stage as

$$\tan(\theta) = \frac{g_Y}{g_L}, \tag{2.39}$$

similarly to the SM. All couplings can be expressed in terms of the electric charge e and the angles:

$$g_L = \frac{e}{\sin(\theta)} \tag{2.40}$$

$$g_R = \frac{e}{\cos(\theta)\sin(\phi)} \tag{2.41}$$

$$g_X = \frac{e}{\cos(\theta)\cos(\phi)}. \tag{2.42}$$

The gauge bosons of the unbroken theory are denoted as

$$SU(2)_L : W_{L,\mu}^{\pm}, W_{L,\mu}^3 \tag{2.43}$$

$$SU(2)_R : W_{R,\mu}^{\pm}, W_{R,\mu}^3 \tag{2.44}$$

$$U(1)_X : X_\mu. \tag{2.45}$$

Some neutral gauge bosons mix after the first stage of symmetry breaking to the neutral gauge states

$$Z_{R,\mu} = \cos(\phi) W^3_{R,\mu} - \sin(\phi) X_\mu \tag{2.46}$$
$$B_\mu = \sin(\phi) W^3_{R,\mu} + \cos(\phi) X_\mu. \tag{2.47}$$

Further neutral gauge boson mixing takes place after the second breaking stage

$$Z_\mu = \cos(\theta) W^3_{L,\mu} - \sin(\theta)\sin(\phi) W^3_{R,\mu} - \sin(\theta)\cos(\phi) X_\mu \tag{2.48}$$
$$A_\mu = \sin(\theta) W^3_{L,\mu} + \cos(\theta)\sin(\phi) W^3_{R,\mu} + \cos(\theta)\cos(\phi) X_\mu. \tag{2.49}$$

Altogether the resulting gauge bosons below the electroweak scale are three massive gauge bosons $W^\pm_{R,\mu}$ and Z_R, that couple only to right-handed fermions, three massive gauge bosons $W^\pm_{L,\mu}$ and Z_L, that couple only to left-handed fermions and the massless photon A_μ that couples to all charged fermions. $W^\pm_{L,\mu}$ and $W^\pm_{R,\mu}$ as well as Z_L and Z_R mix in principle after the second breaking stage. Since already existing limits on the W_R mass enforce $u_T \gg v$, it is possible to neglect this mixing as well as all its effects on the interactions up to leading order in $\frac{v^2}{u_T^2}$ [20].

We use the same parametrization like in [20], where all the new interactions that are relevant here, are parametrized by $\cos\phi$, $\sin 2\beta$ and the ratio of the two VEVs $x = \frac{u_T^2}{v^2}$.

In this parametrization the Higgs VEV v of the second breaking stage is

$$v = \sqrt{\frac{1}{\sqrt{2} G_F}\left(1 + \frac{\sin^2(2\beta)}{2x}\right)} \tag{2.50}$$

with the Fermi constant G_F. The $U(1)_Y$-$SU(2)_L$ mixing angle θ is determined by

$$\sin(2\theta) = \sqrt{\frac{4\pi\alpha_E}{\sqrt{2} M_Z^2 G_F}\left(1 - \frac{1}{x}\left(\frac{\cos^4(\phi)}{4} - \frac{\sin^2(2\beta)}{2}\right)\right)}, \tag{2.51}$$

where α_E is the fine structure constant. The mass of the gauge bosons are (neglecting the contributions of the W_R-W mixing)

$$M_{W_R} = \sqrt{\frac{1}{2} g_R^2 v^2 \left(x + \frac{1}{2}\right)} \tag{2.52}$$
$$M_{Z_R} = \sqrt{x v^2 \left(g_R^2 + g_X^2\right) + \frac{1}{4}\cos^2(\phi) g_R^2 v^2} \tag{2.53}$$
$$M_W = \frac{ev}{2\sin(\theta)}\left(1 - \frac{\sin^2(\beta)}{4x}\right). \tag{2.54}$$

Chapter 3

Recasting of CMS-EXO-13-008

This chapter describes the reconstruction of the CMS-Analysis "Search for heavy neutrinos and W_R bosons with right-handed couplings in a left-right symmetric model in pp collisions at $\sqrt{s} = 8\,\text{TeV}$" [9] (CMS-EXO-13-008) beginning with a description of the analysis. Following in the later sections is the description of the event generation, the detector simulation and the Implementation of the event analysis itself.

1 CMS-EXO-13-008

The CMS-EXO-13-008 analysis is designed for the search for heavy neutrinos and W_R bosons in left-right symmetric extensions of the standard model. In this analysis a simplified LR model is studied to set limits on the mass of the right-handed W boson M_{W_R} and the mass of the right-handed neutrino M_{N_l}. The gauge bosons $W_R^\pm$ are introduced independently of the symmetry breaking mechanism and the Higgs representation. Their mass M_{W_R} is a free parameter as well as the mass of the right-handed neutrino. Additionally strict left-right symmetry at the scale M_{W_R}, which implies $g_R = g_L$, small mixing between the bosons of left and right-handed interactions and identical mixing matrices for left and right-handed quarks and neutrinos are assumed. One predicted process that could occur at the LHC, if a W_R and a right-handed Majorana neutrino exist, is

$$p\ p \to W_R^\pm \to N_l\ l^\pm \to l^\pm\ l^\pm\ j\ j. \tag{3.1}$$

It was first pointed out in [31] as a clean and easily detectable signal in LR models, which has no missing energy. The process is therefore sometimes called Keung-Senjanovič (KS) process and was also studied in [30, 32]. Possible Feynman diagrams for the hard process are shown in figure 3.1.

In this process first a heavy $\mathrm{W_R^\pm}$ is produced, which then decays into a lepton l and a right-handed neutrino N_l with the flavour l. Obviously only the case $M_{\mathrm{W}_R} > M_{\mathrm{N_R}}$ is considered here, although this is not restricted by the model and could vary independently. Because of the assumption of a small mixing between leptons and the small mixing between the left

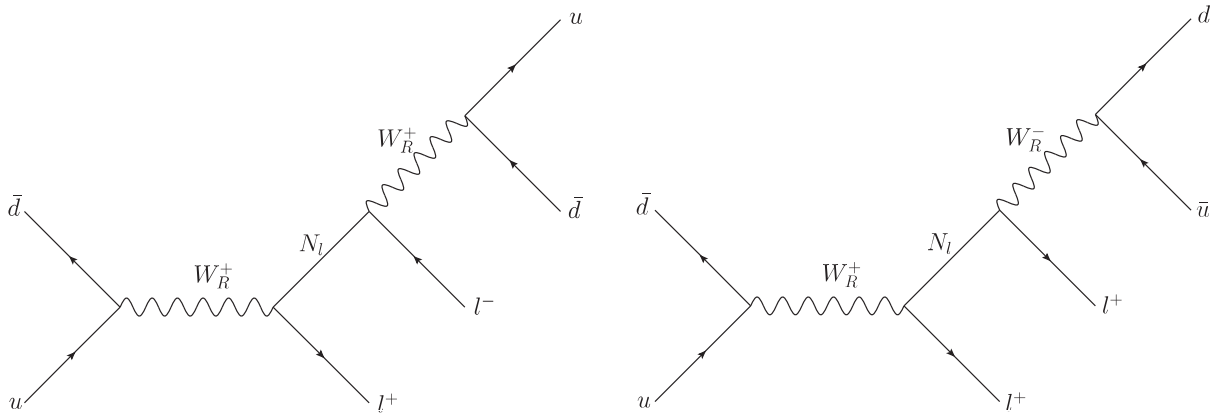

Figure 3.1: two possible Feynman diagrams for the hard scattering of process (3.1)

and right-handed bosons, the heavy neutrino and the lepton are right-handed and have the same flavour.

At LO the averaged squared matrix element for the production of one heavy right-handed neutrino and one lepton is:

$$|\overline{M}|^2 = \frac{1}{3}\frac{1}{s - M_{W_R}^2}|c_{lN_l}|^2|c_{q\bar{q}}|^2 u(u - M_{N_l}^2) \tag{3.2}$$

using $c_{q\bar{q}}\gamma^\mu P_R$ and $c_{lN_l}\gamma^\mu P_R$ as general couplings for the vertices $q\ \bar{q}\ W_R$ and $N_l\ l\ W_R$. Here t, u and s are the Mandelstam variables and all masses except the right-handed neutrino and gauge boson mass were neglected. The colour factor for this process is 3 and the final state averaging over the unobserved degrees of freedom in the initial state gives a factor of $\frac{1}{36}$.

In the next step the right-handed neutrino decays via a virtual $\mathrm{W_R^\pm}$ to a lepton of the same flavour and two quarks. Thus, the observable final state consists of two leptons of the same flavour and two jets j, if no wide-angle emission occurs.

Due to the Majorana nature of the heavy neutrinos in LR-models, lepton flavour violating processes can occur and the two final state leptons can have the same electric charge (see the right diagram of figure 3.1 as an example). Therefore the charge of the final state leptons is ignored and only the flavour is considered in this analysis.

CMS studies three different scenarios for the masses of the right-handed neutrinos.

First the case where only one right-handed neutrino flavour is light enough to contribute to the decay width of the $\mathrm{W_R^\pm}$, is considered. The light neutrino here is either the electron or the muon neutrino. This results in a signal where only electrons or muons are produced by the W_R, which are called electron or muon events, respectively. Since the masses of electrons and muons are negligible, the cross sections are the same and only the detector can lead to different event numbers.

In the last scenario all right-handed neutrinos have the same mass and the considered signal consists of electron and muon events.

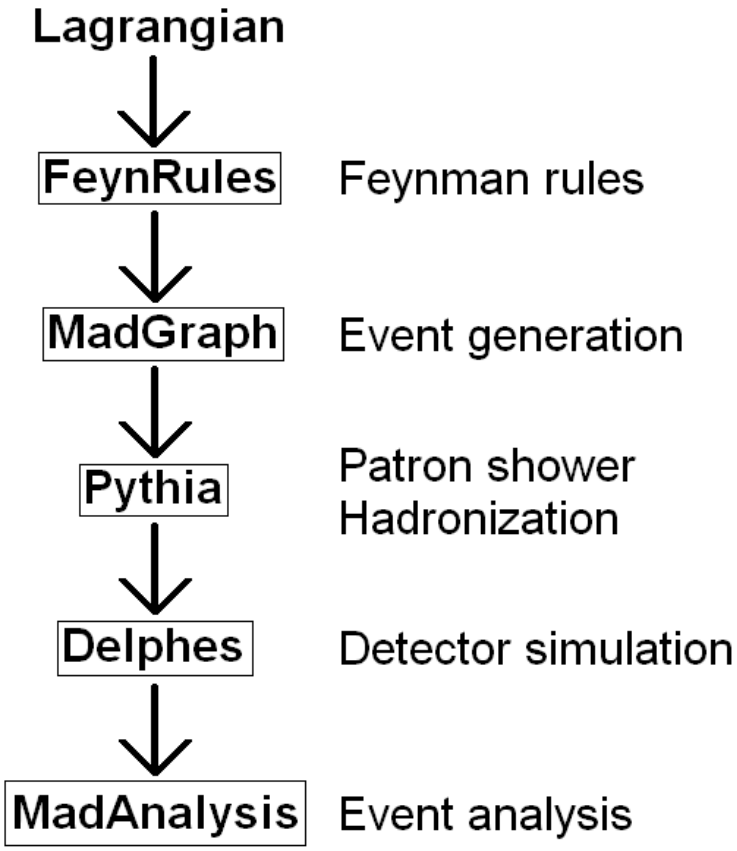

Figure 3.2: Schematic overview of the used programs

The CMS analysis uses NNLO cross sections calculated with FEWZ [33] and event samples generated with pythia 6.4.26 [15] using CTEQ6L1 parton distribution functions [34] and the event tune Z2* [35]. For $M_{N_l} = \frac{M_{W_R}}{2}$ event samples a full CMS detector simulation based on GEANT4 [36] was applied, while the W_R boson production cross section limits for $M_{N_l} \neq \frac{M_{W_R}}{2}$ were computed with event samples without the fully simulated detector response.

Here we use MadGraph5 2.3.2.2 [17] as event generator with a left-right supersymmetric model (LRMSSM) file [19], that was implemented via the UFO file format [37]. Parton showering was taken into account with the Pythia-pgs package [16]. The simulation of the detector response was done with DelphesMA5tune [38] while the analysis itself was implemented in MadAnalysis 5 (MA5) 1.1.12.17 [39, 40]. The CMS-Analysis CMS-EXO-13-008 was reproduced in the context of the MadAnalysis5 Public Analysis Database (PAD) for recasting LHC results [38, 41]. A schematic overview of the used programs is shown in figure 3.2.

label	$M_{N_e} < M_{W_R}$	$M_{N_\mu} < M_{W_R}$	$M_{N_e} = M_{N_\mu} = M_{N_\tau} < M_{W_R}$
l	*e+ e-*	*mu+ mu-*	*mu+ mu- e+ e-*
nl	*ne*	*nm*	*ne nm*

Table 3.1: Definitions of the different multi particle labels for MadGraph

2 Event generation

MadGraph5 2.3.2.2 was used as event generator. The analysed models were implemented with the help of FeynRules 2.1 [42]. FeynRules is a Mathematica package that utilises a so called model file as input to calculate the Feynman Rules of a specific model. In order to implement a model one has to write the Lagrangian and all definitions of fields, parameters and gauge groups in a model file. An explanation how to express everything that has to be provided via a model file, is given in [42, 43]. The computed Feynman Rules were then implemented via the UFO format in MadGraph.

For the validation the employed model file was a left-right supersymmetric model with decoupled supersymmetric particles. To check the implementation, the calculated cross sections and the model file itself were compared with an independent implementation of the LR model [44]. Due to this cross check two errors were found in the left-right supersymmetric model file. The first one was a mistake in the definition of the CKM matrix. It was defined as the real part of the matrix plus the real part times the imaginary unit i instead of the real part of the matrix plus the imaginary part times i. The second bug was the definition of the neutrinos as fermions and not as Majorana particles.

Once the model is implemented MadEvent is created for the specific process via the console of MadGraph. In MadGraph-syntax the production of a right-handed Neutrino and a lepton via a W_R and the decay looks like:

$$p\ p\ >\ l\ nl,\ nl\ >\ l\ j\ j \tag{3.3}$$

Here l and nl are multi particle labels that differ for each of the three right-handed neutrino mass scenarios and j is the predefined multi particle label for jets. l is the multi particle label for the produced leptons and has to be defined as the lepton and its antiparticle to account for the possible Majorana nature of the right-handed neutrino. The right-handed neutrino is the multi particle label nl and its definition is determined by the specific mass neutrino scenario. It can be the right-handed muon neutrino for muon events ($l =$ *mu+ mu-*), the right-handed electron neutrino for electron events ($l =$ *e+ e-*) or both for degenerated neutrino masses ($l =$ *mu+ mu- e+ e-*). The flavour of the right-handed neutrino fixes already all possible processes, if there is no mixing between the different neutrino flavours. Thus, it is also possible to use the definition $l =$ *mu+ mu- e+ e-* for all three scenarios.

An overview of all multi particle definitions is given in table 3.1.

The event generation was speeded up with the option to use a restriction file in MadGraph [17]. Here a BSM-LHA file, which is also called parameter card in the context of MadGraph, was used as restriction-file. All parameters and masses were adjusted to fulfil the assumptions mentioned before like strict LR-symmetry ($g_R = g_L$). Additionally, the supersymmetric

particles had to be removed and the Higgs sector had to be neglected. Subsequently all supersymmetric and Higgs particles were decoupled by setting their masses to a higher scale than the $W_R^{\pm}$ mass. The CKM matrix was set to unity and the mixing between neutrinos was also neglected.

After creating MadEvent with this restriction-file, the input files of MadEvent were modified. The decay widths of particles involved in the process had to be provided in the parameter card. For this analysis only the widths of W_R and of the right-handed neutrino were needed. They were calculated with the Auto-Decay Computation of MadEvent with the command "compute widths" followed by the list of all needed particles. The other option to use the Auto-Decay Computation is the replacement of the width with "Auto" in the parameter card. Unfortunately this option had a bug that crashed MadEvent. All Auto Decay computations are only valid in the narrow width approximation, which is justified here because all masses are much bigger than the widths.

For the event generation the standard run card of MadGraph with a different centre of mass energy $\sqrt{s} = 8\,\text{TeV}$ and the CTEQ6L1 parton distribution functions implemented with LHAPDF [45] were used.

Parton showering and hadronization were performed with the MadGraph package Pythia-pgs which uses Pythia 6.4.28. To be consistent with the CMS collaboration Pythia was run in the Z2 tune.

The errors of the cross sections obtained by the event generator are not considered because of the later use of a k-factor to compare the LO with the NNLO results of CMS.

3 Detector simulation

Since no detector is perfect, the properties of the detector must be taken into account. One limitation of the detector is that the final state particles of an event can fly past the detector and will therefore not be detected. There is also always the possibility that a particle is misidentified or can not be identified because of incomplete data. All kinematic properties of a particle can only be measured with a certain precision, and the detector itself is not homogeneous either. Effects such as these result in different efficiencies and resolutions that depend on the particle itself, the part of the detector where the particle flies through and also on momentum and energy of the particle. This section provides first a short description of the CMS detector, and then the implementation and simulation of its effects is depicted and specified.

3.1 CMS-detector

The following short overview is based on [12], where a much more detailed discussion of the detector is available.

The Compact Muon Solenoid (CMS) is a multi-purpose detector at the Large Hadron Collider (LHC). It is designed to measure the energy and momentum of collisions products like charged leptons, hadrons and photons. For this purpose the CMS detector consists of different layers around the interaction point. The first layer consists of a pixel and a silicon tracker. Its acceptance ranges up to $|\eta| < 2.4$. The second layer is an electromagnetic calorimeter (ECAL) for electrons and photons followed by a hadron calorimeter. The ECAL consists of the barrel, which covers $|\eta| < 1.479$, and the end cap, which covers $1.479 < |\eta| < 3.0$. These parts are enclosed by a superconducting solenoid, which is used to generate a strong magnetic field. The last layer is the muon detector. Because of the high luminosity and the high rate of events per second the online event selection process ("trigger") must reduce the number of events for storage and following analysis.

3.2 Implementation in DelphesMA5tune

To respect the effects of the CMS detector on the outcome of the analysis the MadAnalysis package DelphesMA5tune [38] based on Delphes 3 [46] was used. This fast detector response simulation is not a full CMS detector simulation like the one used by [9], which is based on GEANT4. With DelphesMA5tune the response of the detector to an event is simulated by efficiencies and resolutions to detect a specific type of particle or one of its properties. In order to run DelphesMA5tune these information have to be provided via a DelphesMA5tune card.

Because of the simplifications of the fast detector response simulation differences of 20% between a full and a fast detector simulation are expected in general [38, 41]. There is also no estimation of simulation errors like in a full detector simulation.

Here a CMS DelphesMA5tune card, based on the card [47] available through the PAD, was used, where the efficiency and tracking efficiency for muons and electrons were modified. The needed efficiencies for muons and electrons were set in the Delphes card accordingly to [48] and the preliminary CMS-results available online [49, 50, 51]. All of them are depending on the rapidity and transverse momentum of the muon or electron and were measured by the CMS collaboration for the $s = \sqrt{8}$ run. There are two different muon identification efficiencies available, which correspond to the loose and tight muon identification criteria [52]. Tight muon identification efficiencies were used, which is explicit stated in the $s = \sqrt{7}$ search for heavy neutrinos and W_R bosons [10]. They are given in DP2012_025 [50]. The muon tracking efficiency for $|\eta| < 2.4$ was taken from TRK-10-002-pas [49] and for $|\eta| > 2.4$ from [48]. For electrons the tracking efficiency and the identification efficiency are given in CERN-CMS-DP-2013-003 [51]. Like in other analyses [53, 54] the region between the ECAL barrel and the end cap with $1.442 < |\eta| < 1.560$ is not used for the detection of leptons. Figure 3.3 shows the electron identification efficiency for $|\eta| < 0.8$ as an example of a used CMS plot.

In general the efficiencies for leptons grow for larger p_T.

All settings in the card concerning the detector response simulation of jets were left unchanged. As in [9] the anti-k_T clustering algorithm [55] with a distance parameter of 0.5 was

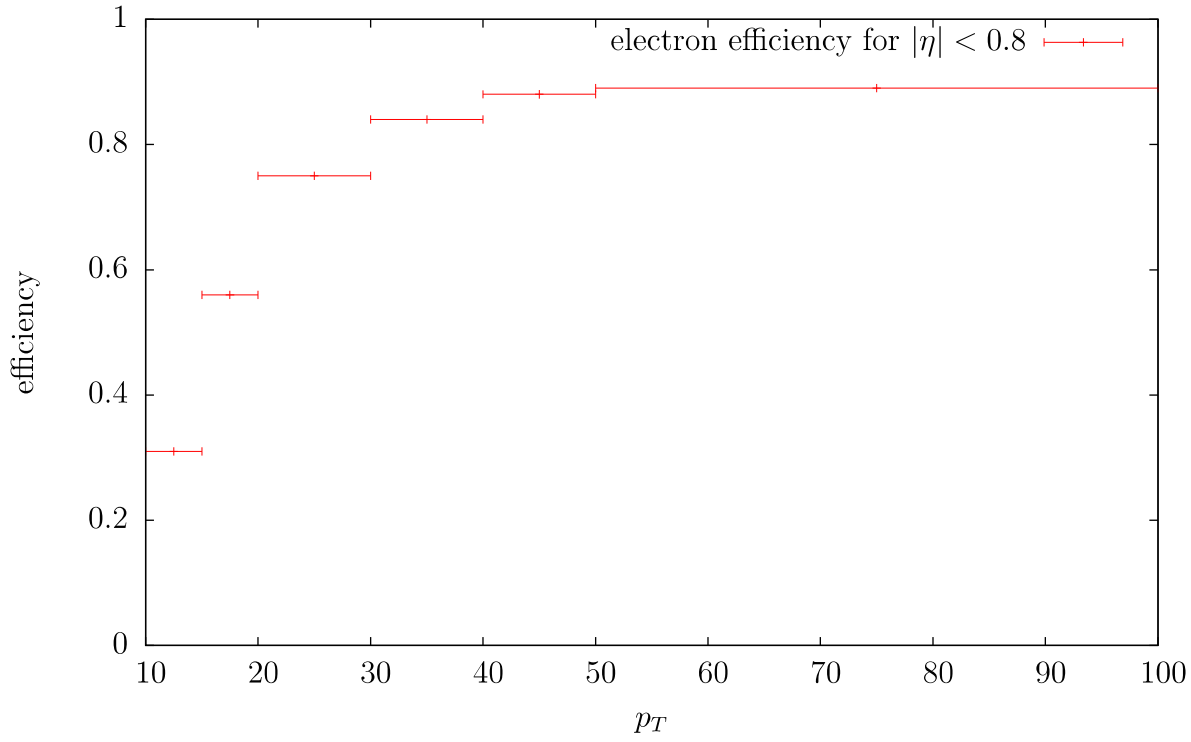

Figure 3.3: Electron identification efficiency for $|\eta| < 0.8$ [51]

used to reconstruct jets. In MadAnalysis the Algorithm is provided by FastJet [56, 57].

The effects of pile up collisions were not considered and not implemented.

4 Event Analysis

The analysis of real or simulated detector output is an essential part of collider physics. After all the final state particles of an event were identified and their properties were measured, it has to be decided which events could originate from the wanted process. The improvement of the signal to background ratio is also an important issue.

Both are done with the help of so called cuts. A cut is just a condition that is imposed and every event, that does not fulfil it, is ignored in the later considerations. For background reduction it is obvious that events, that originate from the considered process, should fulfil this requirement more likely than background processes.

This section first describes the CMS-EXO-13-008 analysis and then its implementation.

4.1 Description

The CMS-EXO-13-008 analysis is designed for the search for heavy neutrinos and heavy W_{R} bosons and thus uses algorithms for objects with large p_{T} [53, 58]. An earlier version of this analysis is described in the $\sqrt{s} = 7\,\mathrm{TeV}$ search [10].

As previously stated the final state of the hard scattering consists of two quarks and two leptons with the same flavour, while there are no requirements for the electric charge of the two leptons. Thus the analysis only takes events with a $eejj + X$ (electron event) or $\mu\mu jj + X$ (muon event) observed final state into account, where both leptons and jets have large p_{T}.

There are different selection requirements imposed to identify possible candidates for this process in the event samples. The first requirements deal with the jets. Because the $\mathrm{W}_{\mathrm{R}}^{\pm}$ has to be heavy, if it exists, it is required that there are at least two jets with $p_{\mathrm{T}} > 40\,\mathrm{GeV}$ in an event candidate. The two jets with the highest p_{T} are then called leading jets.

To exclude leptons that originate from a jet and because the decay products of the W_R are very likely spatial separated, all leptons within a cone of radius $\Delta R < 0.5$ around one of the leading jets are ignored. An additional requirement is imposed to suppress non-isolated muon backgrounds like muons from the decay-in-flight of hadrons. This is realized by computing the sum of the transverse momentum of all tracks within a cone of radius $\Delta R < 0.3$ around a muon track. The muon is ignored, if the sum is larger than 10% of the muon p_{T}. Then it is required that the lepton with the highest p_{T} (leading lepton) satisfies $p_{\mathrm{T}} > 60\,\mathrm{GeV}$, while the same flavour lepton with the next highest p_{T} satisfies $p_{\mathrm{T}} > 40\,\mathrm{GeV}$.

The p_T requirements for the leptons and jets reflect the structure of the W_R decay. Since the W_R and the N_l are believed to be heavy both leptons and both jets will have a large momentum. The lepton directly produced together with the right-handed neutrino will tend to have a larger momentum than the lepton produced by the decay of the neutrino, which leads to the p_T cuts for the leading and sub leading leptons.

There are also conditions for the pseudorapidity of the detected particles. The tracker for charged particles covers $|\eta| < 2.5$, which is why electrons and jets are reconstructed in this η range. Muons can be detected for $|\eta| < 2.4$, but the trigger selects only events with at least one muon, that fulfils $|\eta| < 2.1$.

Hereafter all these conditions combined are called ee or $\mu\mu$ requirements in order to distinguish them from the following cuts, which are imposed to improve the signal to background ratio. In the following sections event numbers for the requirements stage also include all other effects from the detector simulation.

Processes which give the same signal were studied and simulated by CMS with the conclusion that the dominant background processes are Drell-Yan with jet processes $pp \to Z/\gamma\ jj \to lljj$ and $t\bar{t}$ production $t\bar{t} \to bW\bar{b}W \to jjll + \text{neutrinos}$, where the neutrinos can not be detected. Other SM background processes are altogether less than 10% of the whole background. The CMS event numbers for the background are shown in table 3.2.

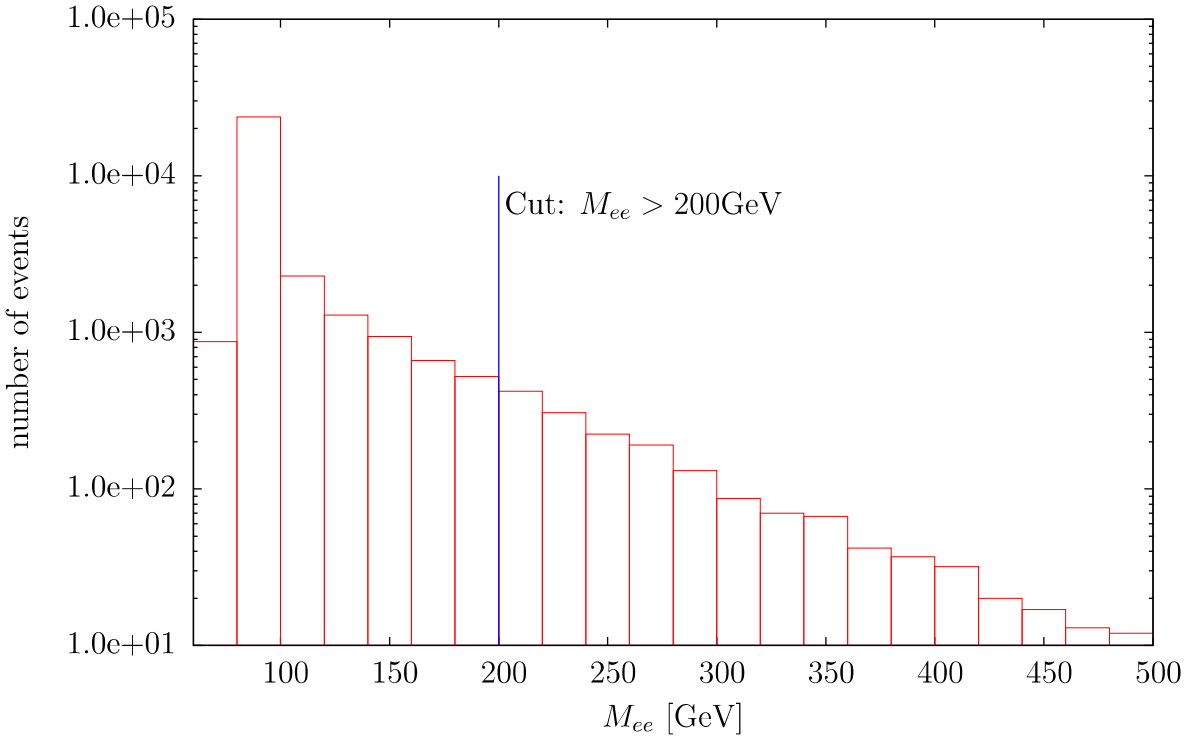

Figure 3.4: CMS M_{ee} distribution of the background and $M_{ee} > 200\,\text{GeV}$ Cut

The reduction of the background events in the CMS $\sqrt{s} = 8\,\text{TeV}$ search is realized by two cuts. For the first cut only events with $M_{ll} > 200\,\text{GeV}$ are considered, while the second cut requires $M_{lljj} > 600\,\text{GeV}$. Both are motivated by the heaviness of the W_R. Especially $M_{ll} > 200\,\text{GeV}$ reduces the Drell-Yan with jet background because W_R is much heavier than a Z boson.

As an example the CMS invariant mass distribution M_{ee} for the background that fulfils the p_T requirements is shown in figure 3.4.

One can see that the number of background events decreases rapidly for larger M_{ee}, which is similar for $M_{\mu\mu}$. The peak at the bin from 80 GeV to 100 GeV is just the Z resonance.

Figure 3.5 shows the distribution of one example W_R-signal, simulated by CMS, in comparison with the simulated background. The example signal was simulated for $2M_{N_l} = M_{W_R} = 2.5\,\text{TeV}$.

Here the different shapes of the signal and background distributions are visible, which is the basic requirement for the $M_{eejj} > 600\,\text{GeV}$ cut. The exact value of the cut is a compromise between the reduction of background events and not cutting away signal events.

Beside the simulated events figure 3.5 also shows the M_{lljj} distribution measured from CMS. A distinctive feature of the measured CMS data is an excess in the electron channel at $M_{eejj} \approx 2\,\text{TeV}$.

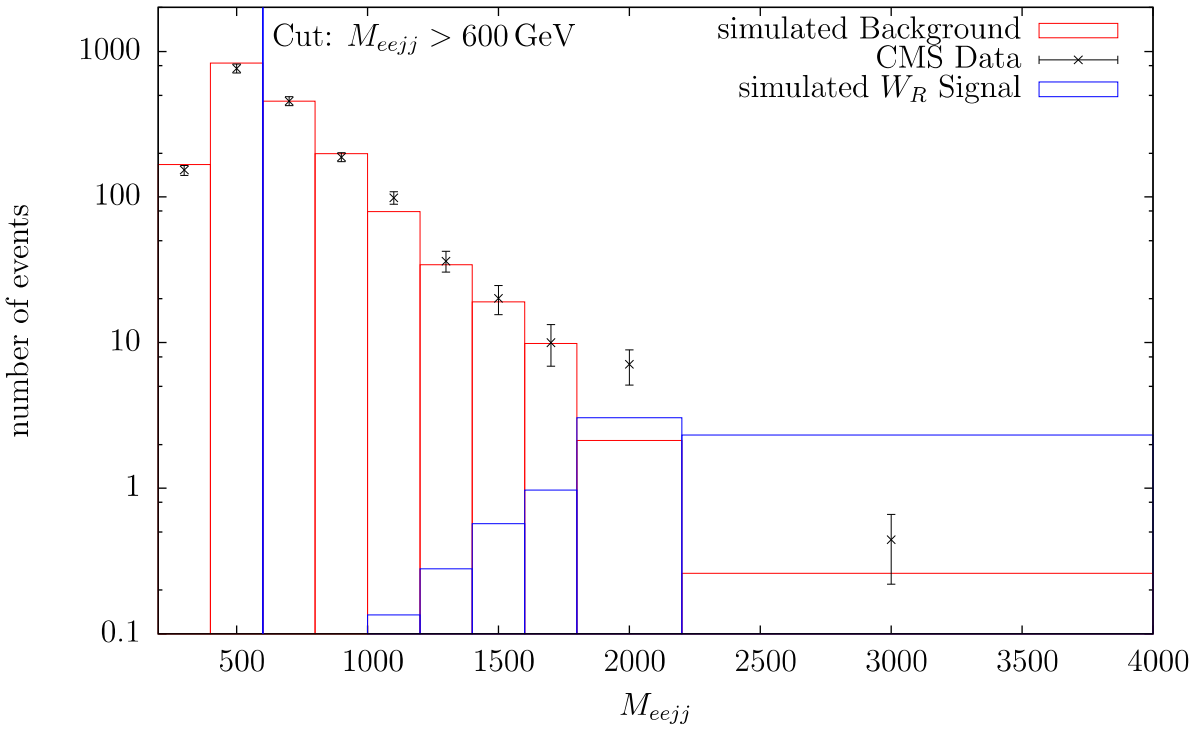

Figure 3.5: CMS M_{eejj} distribution of the background and the W_R signal for $2M_{N_l} = M_{W_R} = 2.5\,\mathrm{TeV}$ and the $M_{eejj} > 600\,\mathrm{GeV}$ Cut

stage	total background	Drell-Yan + Jets	$t\bar{t}$ production	other
ee requirements	34154	28273	4725	1156
$M_{ee} > 200\,\text{GeV}$	1747	475	1164	108
$M_{eejj} > 600\,\text{GeV}$	783 ± 51	252 ± 24	476 ± 42	55 ± 12
$\mu\mu$ requirements	41204	34220	5625	1359
$M_{\mu\mu} > 200\,\text{GeV}$	2064	549	1382	133
$M_{\mu\mu jj} > 600\,\text{GeV}$	913 ± 58	287 ± 26	562 ± 50	64 ± 12

Table 3.2: Standard model backgrounds simulated by CMS ([9] tab.1)

The event numbers from CMS for the different background processes and their reduction by the cuts are given in table 3.2.

4.2 Implementation in MadAnalysis

This section describes the implementation in MadAnalysis, which was used in the Expert mode to analyse the root output files of the detector response simulation. With the expert mode of MadAnalysis it is possible to program a analysis in C++ using the tools that are provided by the SampleAnalyzer library. The self-implemented analysis is then applied to the detector output and produces histograms and a so called cut-flow that gives the number of events that survive each cut. This cut-flow is used to compute the signal acceptance of the analysis and detector simulation. A detailed discussion how to use the expert mode of MadAnalysis can be found in [41].

The user has to program three functions called Initialize, Execute and Finalize in the main file of the analysis.

In the Initialize function all histograms and applied cuts have to be declared. It is executed only once per analysed event file.

The Execute function contains all steps of the analysis like cuts that are automatically applied by MadAnalysis to every event of an analysed event file.

The first part of the Execute routine is the selection and collection of jets and electrons in two distinct temporary storages named containers. To speed the analysis up and to save memory only jets and electrons with $p_T > 40\,\text{GeV}$ and $|\eta| < 2.5$ of one event are stored in containers.

After both containers are filled all electrons have to be removed from the jet container. This is necessary, because contrary to expectations, both electrons and real jets are given by the "event.rec()->jets()" method while the "event.rec()->electrons()" method only gives electrons. The removal of this double counting is performed by the OverlapRemoval function declared in the header. It compares the distance between one element of the first container with one element of the second container and removes the element from the first container, if the distance is too small. This comparison is done for all elements of both containers. Here it deletes every element in the jet container, if an electron is inside a cone of $\Delta R < 0.2$

around the jet. Then the jet container is sorted by p_T and the first cut is applied. Every event with less than two jets is rejected to realise the requirement that there are at least two jets with $p_{\mathrm{T}} > 40\,\mathrm{GeV}$ and $|\eta| < 2.5$ in an event. For the following analysis the two jets with the highest p_T (leading jets) are then stored in a new container.

Next the isolation criteria for electrons are executed. With the OverlapRemoval function all electrons within a cone of $\Delta R < 0.5$ around a leading jet are erased. The electron container is then also sorted by p_T.

The next step is the collection of all muons with $p_T > 40\,\mathrm{GeV}$ and $|\eta| < 2.5$ in a container and the isolation criteria for muons are applied. The first one is the removal of every muon within a cone of $\Delta R < 0.5$ around a leading jet and the second one is the suppression of non-isolated muon backgrounds. Every muon in the container is erased, if the p_T sum of every track within a cone of $\Delta R < 0.3$ around the muon is larger than 10% of the muon p_T.

After all leptons that survive the isolation criteria were stored in the containers and sorted by p_T, the leading leptons have to be identified. To achieve this, two Boolean variables are defined "isEE" and "isMUMU", which show if an event satisfies all criteria for a muon or an electron event. The first criterion to hold for an electron event is at least two electrons with $p_T > 40\,\mathrm{GeV}$ and $|\eta| < 2.5$ in an event, which is checked with the size of the particular container. The second requirement is, that at least one electron satisfies $p_{\mathrm{T}} > 60\,\mathrm{GeV}$. Because the container was sorted by p_T, one has to test $p_{\mathrm{T}} > 60\,\mathrm{GeV}$ only for the first electron in the container. This electron is then called leading electron while the second lepton in the container, which has the second highest p_{T}, is called sub leading electron. Muon events have to fulfil the same criteria as the electron events and also an additional requirement. To be selected by the trigger of the detector at least one muon must have $|\eta| < 2.1$. If the leading muon does not fulfil $|\eta| < 2.1$, all other muons in the container are tested and the sub leading muon is the one that has $|\eta| < 2.1$ instead of the muon with the second highest p_{T}.

In the unlikely case that one event can be counted both as muon event and as electron event, it has to be determined as one of the two possibilities to prevent double counting. Such an event is declared as electron event, if the p_{T}-sum of leading and sub leading electron is larger than the sum of the muons and vice versa.

After the decision, if an event is an electron event, muon event or neither of the two, the cuts are finally applied. Here the events are split into two different so called regions. In general, a region is defined by all the cuts an event has to satisfy to be counted in this region.Thus they grade the events according to some of their properties. Here they are used to distinguish between the two possible signals. One region counts only the number of electron events while the other counts the muon events. Later, these regions are important for the computation of the exclusion limits.

Next the probability that an event passes the triggers is implemented. This trigger efficiency is 99% for electron and 98% for muon events [9]. The weight of an event is multiplied with 0.99 or 0.98 instead of discarding events based on their probability to pass the trigger. Due to this method the statistics obtained from a event file are not downgraded by reducing the number of events.

Then the leading and sub leading leptons are stored in a container for the following calculation of the two and four object mass distributions M_{ll} and M_{lljj}. After the computation of M_{ll} and M_{lljj} the $M_{ll} > 200\,\text{GeV}$ and $M_{lljj} > 600\,\text{GeV}$ cuts are applied.

The last step is the drawing of the M_{ll} and M_{lljj} histograms before and after the $M_{ll} > 200\,\text{GeV}$ and $M_{lljj} > 600\,\text{GeV}$ cuts.

At the end of the file is the Finalize routine, which gives the possibility to program other output formats or diagrams. Since this is not necessary for the analysis, the routine was not modified.

The MadAnalysis source code is given in the appendix.

5 Exclusion limits

The calculation of the exclusion limits was done with the exclusion CLs script [38] available via MadAnalysis. It is based on the CLs prescription [59, 60] which is the same standardized method used by the LHC and CMS. However the exclusion CLs script contains not the full CLs prescription and can not be as detailed as the RooFit and RooStats machinery [61] used by CMS and ATLAS. The exclusion CLs script takes only the total number of events that survive the cuts into account, while the full CMS analysis is shape based and uses multiple bins of the M_{lljj} distribution. Since only the total number of events is published and it is not sufficient to read the background event numbers from a diagram with a log-scale, a shape based analysis is not possible and the employed script is enough. For a more restricting analysis more informations about the SM background and the measured data would be needed.

To run the exclusion CLs script a xml file is needed where the different regions that occur in the analysis are defined. For each of the signal regions the number of events that were measured for this region, the number of background events that is expected and the uncertainty of the background have to be specified in the xml file. Here we use the SM backgrounds given in table 1 in [9], which are also shown in table 3.2. The script can then calculate the CLs exclusion limits and decides which region gives the best limits.

6 Validation

In this section the implementation of the whole analysis from the event generation to the exclusion limits are compared with the results from CMS.

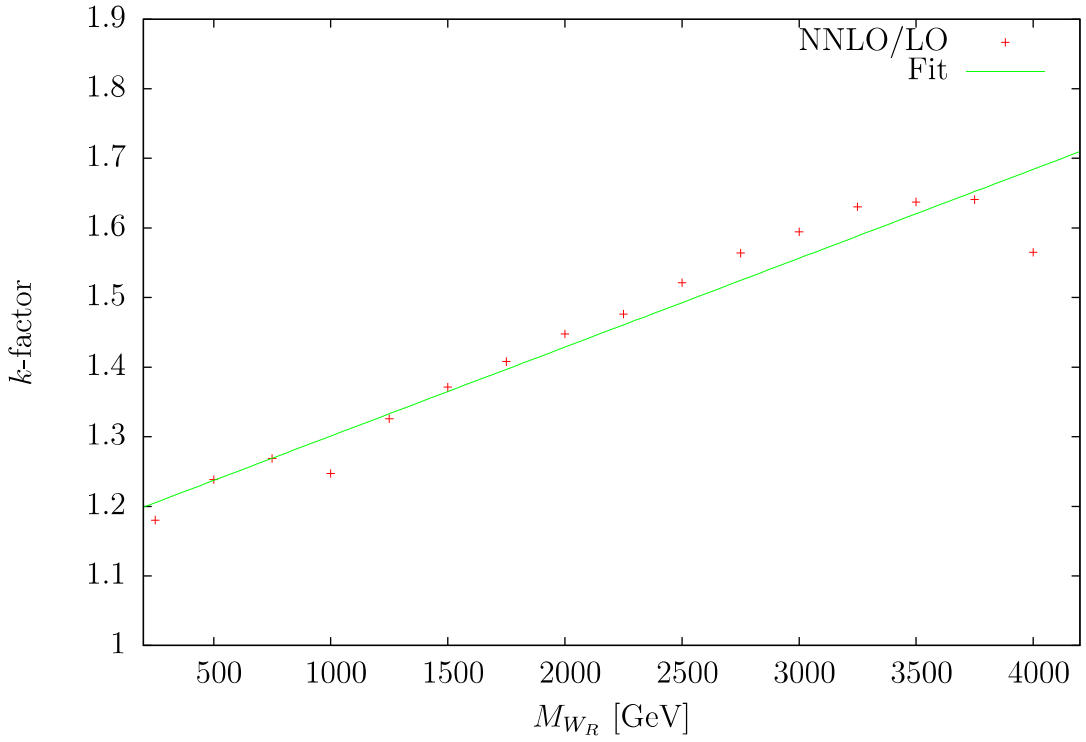

Figure 3.6: k-factors for $M_{W_R} = 250$ GeV to $M_{W_R} = 4000\,\text{GeV}$ calculated with FEWZ

6.1 k-factor

Since NNLO cross sections, calculated with FEWZ, were used by CMS, it is necessary to introduce a k-factor to be able to compare them with the LO-results from MadGraph. Here the k-factor is estimated by calculating the ratio of the NNLO and the LO $W^{\pm}$ production cross sections from FEWZ. The $W^{\pm}$ production cross sections with $M_{W^{\pm}} = M_{W_R}$ can be used here because of the assumption of strict left-right symmetry. It turns out that the k-factor in this case depends mainly on the $W^{\pm}$ mass. Hence, the k-factor was calculated for different W_R masses and then fitted linearly 3.6.

The errors of the fit are not considered here, because the k-factor itself is only an estimation and there is no possibility to estimate the simulation error of the detector response simulation. In the following calculations the used k-factor is computed with this linear fit:

$$k = 0.000128 \cdot M_{W_R} + 1.17336 \tag{3.4}$$

In this analysis, a direct use of FEWZ NNLO cross sections like in the CMS paper is discarded, because we have to validate the LO event files which are used for the detector response simulation, and also the detector response simulation itself.

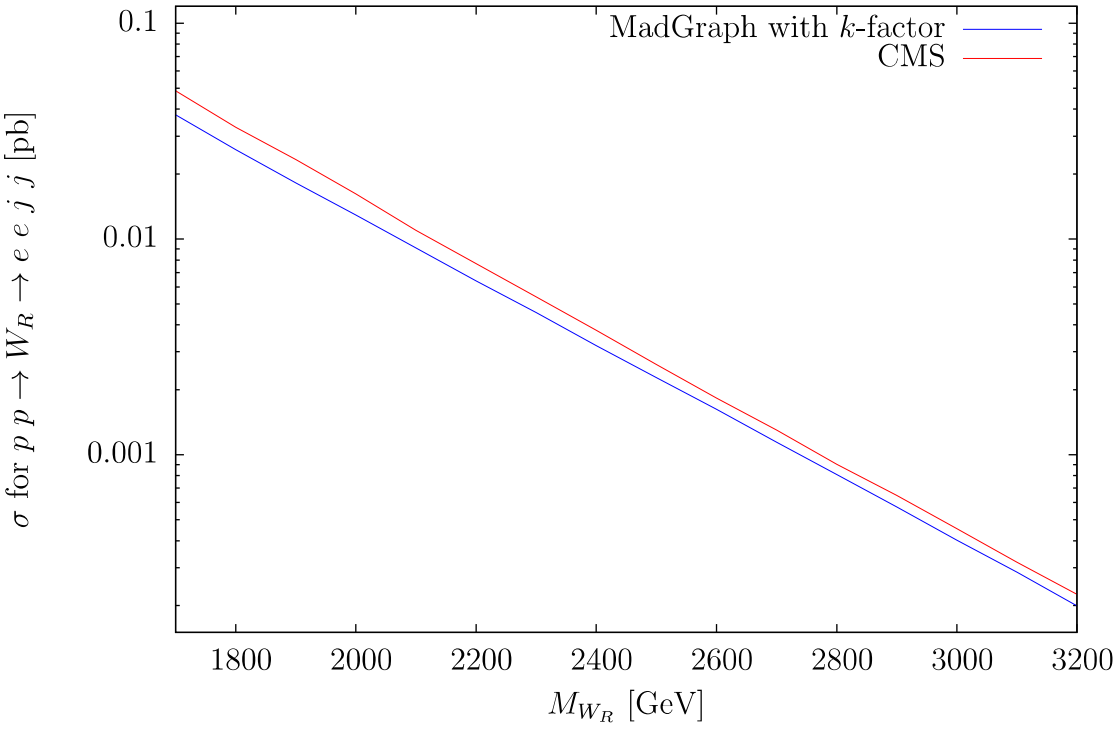

Figure 3.7: Comparison of cross sections for $M_{N_e} = \frac{M_{W_R}}{2}$ and $M_{N_e} < M_{W_R} < M_{N_\mu}, M_{N_\tau}$

6.2 Cross section

Here the CMS cross sections, given in [9] figures 4 and 5, for the first scenario with $M_{N_e} = \frac{M_{W_R}}{2}$ and the second scenario with $M_{N_\mu} = \frac{M_{W_R}}{2}$ are compared with the cross sections calculated with MadGraph. The third scenario with $M_{N_e} = M_{N_\mu} = M_{N_\tau} = \frac{M_{W_R}}{2}$ is also considered.

Figure 3.7 shows the comparison for $M_{N_e} = \frac{M_{W_R}}{2}$ between $M_{W_R} = 1.5\,\text{TeV}$ and $M_{W_R} = 3.2\,\text{TeV}$ (the muon cross sections for $M_{N_\mu} = \frac{M_{W_R}}{2}$ can be found in the appendix 6.1).

The cross sections for electron and muon events are the same as expected. MadGraph gives a curve with a similar shape, but the cross sections are always smaller than the CMS cross sections. This deviation increases for lower M_{W_R} and ranges from $2.5 \cdot 10^{-5}\,\text{pb}$ for $M_{W_R} = 3000\,\text{GeV}$ up to $0.025\,\text{pb}$ for $M_{W_R} = 1500\,\text{GeV}$. In figure 3.8 is the case $M_{N_e} = M_{N_\mu} = M_{N_\tau} = \frac{M_{W_R}}{2}$ pictured.

Figure 3.8 shows exactly the same behaviour as both cases before, but the cross sections are overall larger, which is caused by the new decay channels for the W_R. The branching ratio $W_R \to N_e$ or N_μ for $M_{N_e} = M_{N_\mu} = M_{N_\tau} = \frac{M_{W_R}}{2}$ is larger than the branching ratio $W_R \to N_e$ for $M_{N_e} = \frac{M_{W_R}}{2}$ and $M_{N_e} < M_{W_R} < M_{N_\mu}, M_{N_\tau}$. This effect would be even larger, if the W_R could not decay to a N_τ and a τ, because it is rather unlikely that their decay produces two

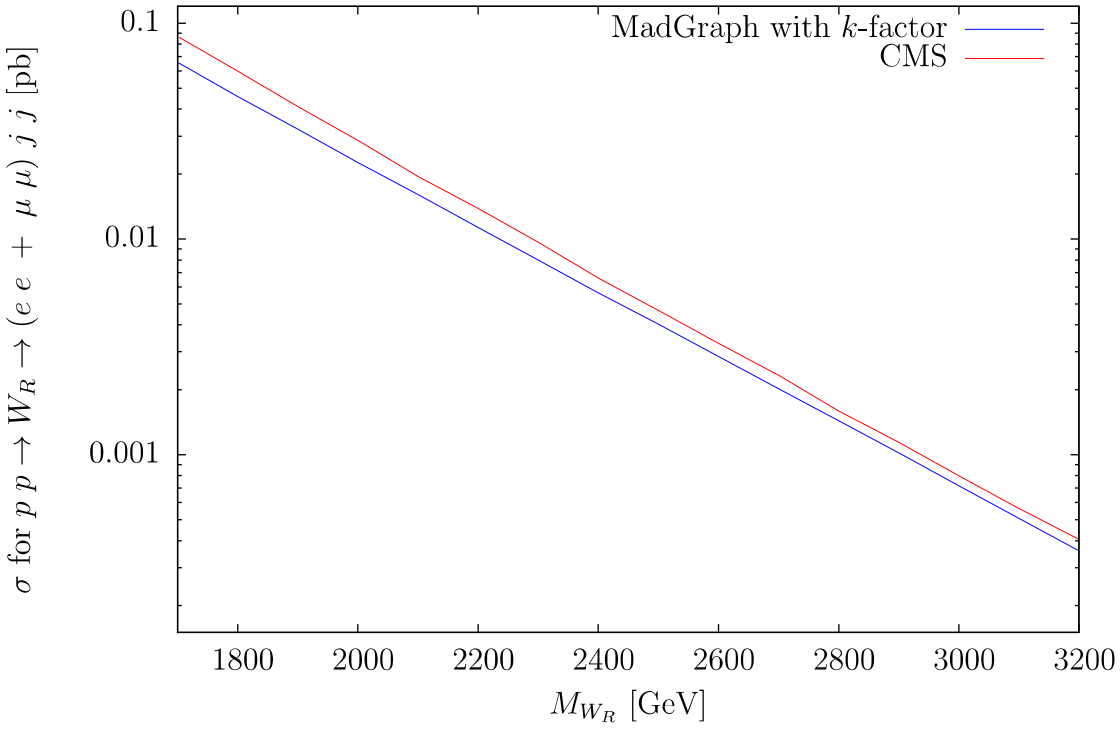

Figure 3.8: Comparison of cross sections for $M_{N_e} = M_{N_\mu} = M_{N_\tau} = \frac{M_{W_R}}{2}$

jets and two same flavour leptons. Even if they produce the needed signal, there would be missing energy due to the produced neutrinos.

The statistical and numerical errors of the MadGraph cross sections are of the order of 10^{-6} or 10^{-7} pb. PDF errors are not calculated because of the LO calculation with a k-factor and LO PDFs.

There are several possible reasons for the cross section discrepancy. First the k-factor itself can only be a rough estimation of a real NNLO calculation. A second issue lies with used programs. Since the cross sections were calculated with two different programs and the exact settings of FEWZ, that was used by CMS, are unknown, it was not possible to reproduce the exact cross sections. The fit of the k-factor itself can be excluded as the root of the discrepancy. Comparisons between k-factors calculated by the ratio $\frac{NNLO}{LO}$ and k-factors obtained by the fit show that the difference of cross section times first k-factor and cross section times second k-factor is of the same order as the error of the cross section.

Altogether the implementation in MadGraph seems to be validated. Although the cross sections are smaller, they still have the same order of magnitude and the same behaviour.

A second k-factor $k_2 = \frac{\sigma_{CMS}}{\sigma_{own}}$ is introduced to estimate the CMS cross section for the later analysis. The fit is shown in figure 3.9 and a linear fit gives

$$k_2 = -0.000134 \cdot M_{W_R} + 1.51356. \tag{3.5}$$

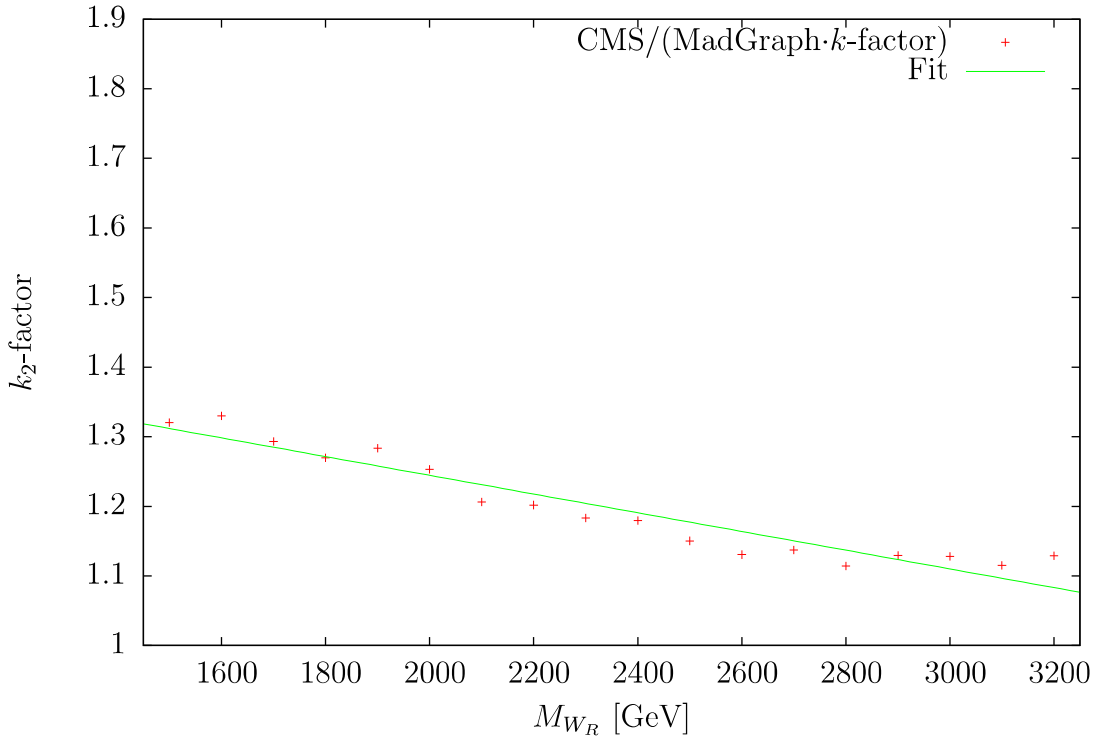

Figure 3.9: $k_2 = \frac{\sigma_{CMS}}{k\sigma_{LO}}$-factors for $M_{W_R} = 1500$ GeV to $M_{W_R} = 3200\,\text{GeV}$

k_2 could only be calculated for $M_{N_l} = \frac{M_{W_R}}{2}$, since this are the only given cross sections in the paper. They are later also used for $M_{N_l} \neq \frac{M_{W_R}}{2}$ assuming, that the M_{N_l} dependence is negligible for k_2.

6.3 Signal acceptance

Now the detector response simulation is checked against the full detector simulation of CMS. In order to do this, the signal acceptance given in the tables in the appendix of [9] is compared with the signal acceptance computed with DelphesMA5tune. Here the signal acceptance is the ratio of the number of simulated W_R-decay events that are counted as signal after detector simulation and event analysis to the total number of simulated W_R-decay events. In figure 3.10(top) is the CMS signal acceptance for different values of M_{W_R} and M_{N_μ} in the second scenario $M_{N_\mu} < M_{W_R} < M_{N_e}, M_{N_\tau}$ shown (the CMS signal acceptance for the first scenario $M_{N_e} < M_{W_R} < M_{N_\mu}, M_{N_\tau}$ is given in the appendix figure 6.2).

The signal acceptance ranges from 35% up to 80% and varies by 1% between electron and muon events [9]. To discuss the physics behind the differences in the acceptance the muon event signal acceptance is plotted as a heatmap 3.10(bottom). A heatmap for electron events can be found in the appendix figure 6.4, which does not show relevant differences for the following discussion.

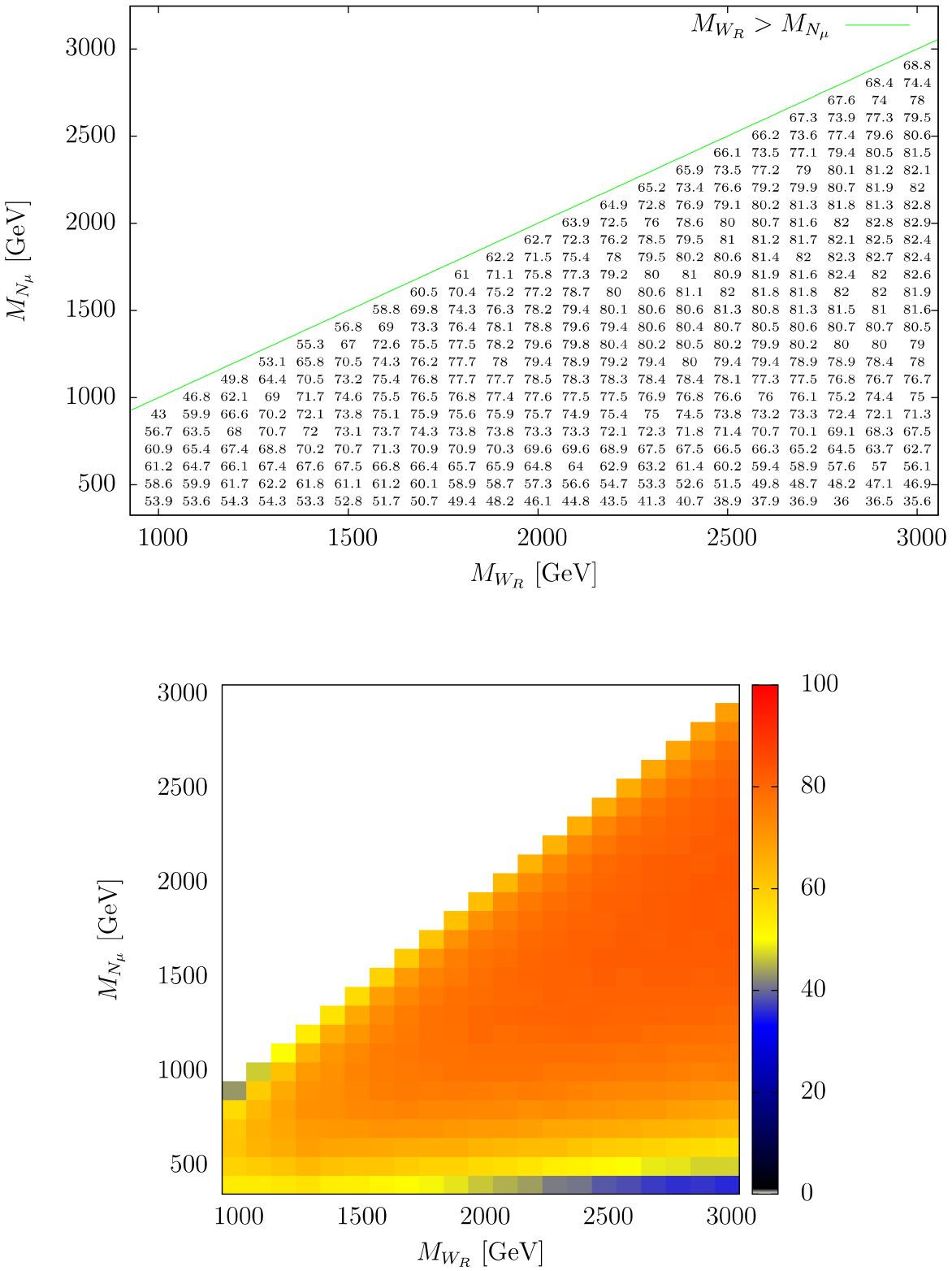

Figure 3.10: CMS signal acceptance for muon events [%](top) and as heatmap [%](bottom)

A general trend is the rise of the acceptance for higher M_{W_R} and M_{N_l}, which is the result of the larger detector efficiencies for increasing p_T of the leptons. One exception is the region of large M_{W_R} and small M_{N_l}, where the signal acceptance drops below 40%. The probability to identify a W_R decay in this analysis depends on the ability to reconstruct all high energetic final state particles. This is only possible if the leptons and jets do not overlap. For the case of $M_{W_R} >> M_{N_l}$ the right-handed neutrino has a high 3-momentum, which in many cases results in small angles between the trajectories of the three decay products ljj in the lab frame. Because of this, the leptons have a high probability to be inside the jet cone. The jets are also close to each other and can be interpreted as one jet in the reconstruction process. Thus, the signal acceptance is reduced in this case [9].

Another trend is the slightly reduced acceptance for large M_{N_l}, which is caused by the lower p_T of the lepton that is produced together with the N_l.

The signal acceptance resulting from the simulation with DelphesMA5tune for muon events is shown in figure 3.11(top) (the electron event signal acceptance is again in the appendix figure 6.3).

They have the same general behaviour like the corresponding CMS acceptance, which can also be seen in the heatmap 3.11(bottom) for muon events, but the acceptance calculated with DelphesMA5tune is almost exclusively smaller than the CMS acceptance.

The ratio of the acceptance computed with Delphes and the corresponding CMS acceptance is shown in figure 3.12 and figure 3.13.

For an easier analysis of the deviation are heatmaps of the MA5/CMS ratios given in 3.14 and 3.15.

The signal acceptance for electrons differs more from the CMS acceptance than the muon acceptance. On average the difference between MA5 and CMS is 16.2% for electron and 8.6% for muon events, which is better than the 20% deviation expected of a fast detector response simulation. The difference between the electron and the muon channel is probably caused by the electron efficiency of the DelphesMA5tune card, which was not as detailed as the muon efficiency for $p_T > 50\,\text{GeV}$. Since the high p_T region is the relevant region for this analysis, detailed electron efficiency data could reduce the differences to a similar level than the muon acceptance. Another issue that could result in an overall discrepancy is the part of the DelphesMA5tune card for jets like the charged hadron tracking efficiency, which was not considered in this work.

In both cases the structure of the deviations is very similar, which suggests there may be issues that are independent of the implementation of the lepton detection. The best agreement is in the region with $M_{W_R} >> M_{N_l}$, which is very close to the CMS result. This is not surprising because the signal acceptance there is dominated by the effect of overlapping jets and leptons and not by the properties of the detector. For reasons that are yet unknown, the region with M_{N_l} close to M_{W_R} has the largest deviation from CMS.

Overall the signal acceptance is in agreement with the given CMS acceptance from a fast-simulation viewpoint and has also the same shape.

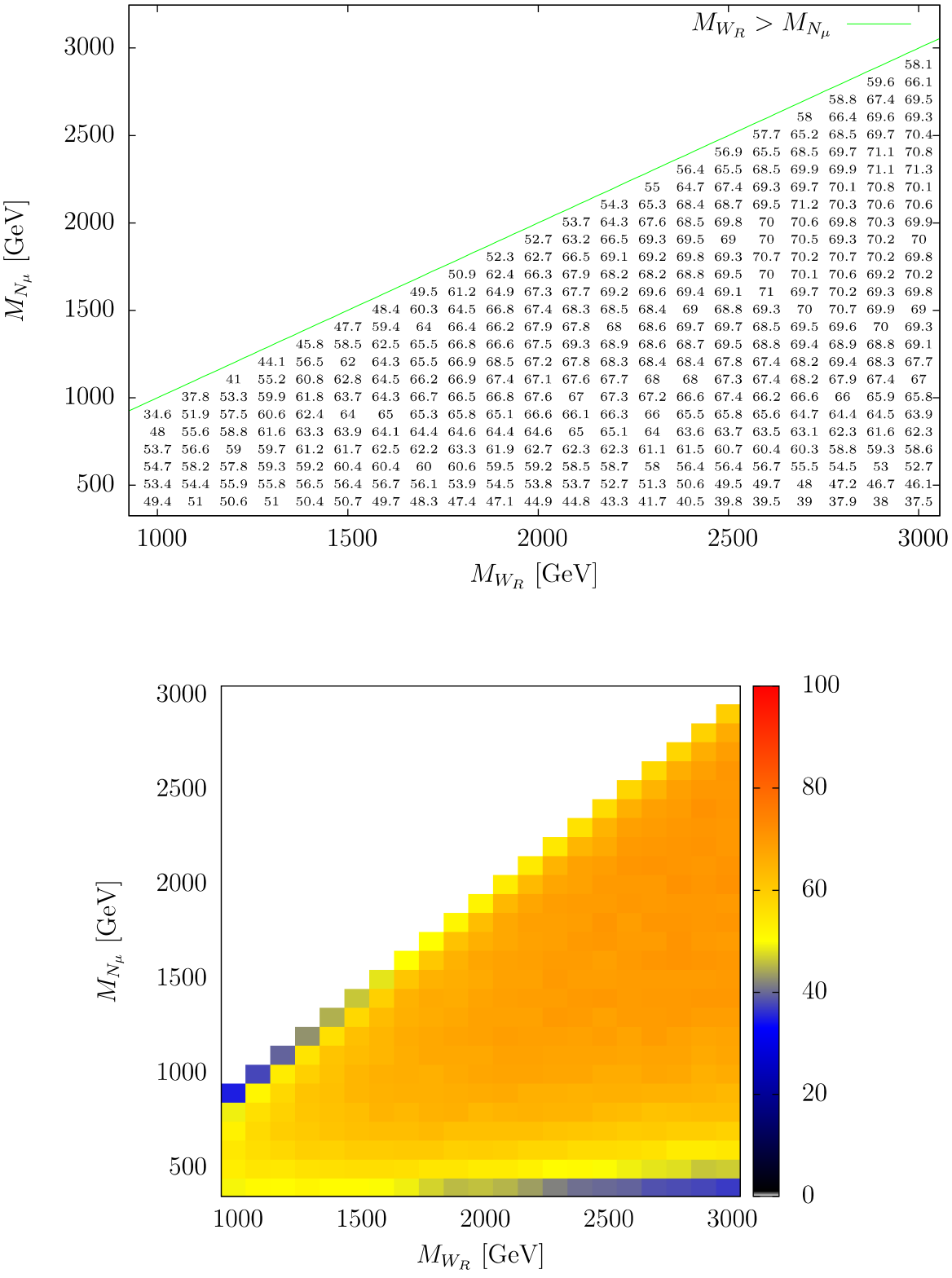

Figure 3.11: Muon event acceptance calculated with DelphesMA5tune [%](top) and as heatmap [%](bottom)

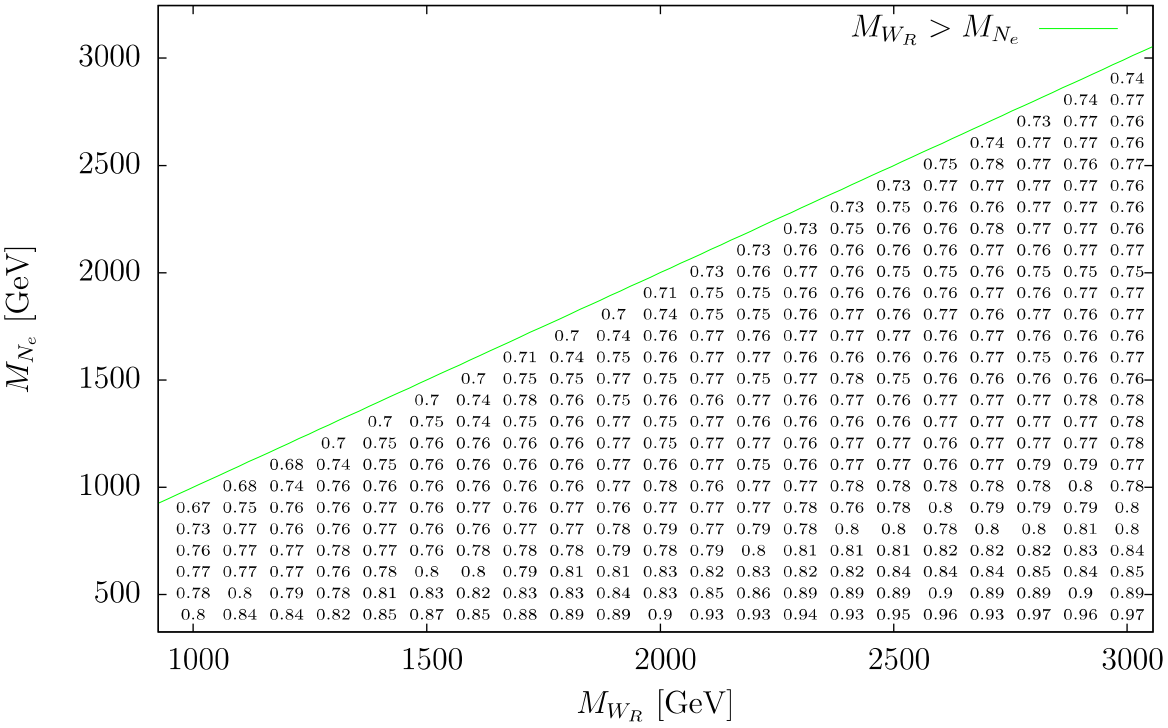

Figure 3.12: Ratio MA5/CMS for electron event acceptance

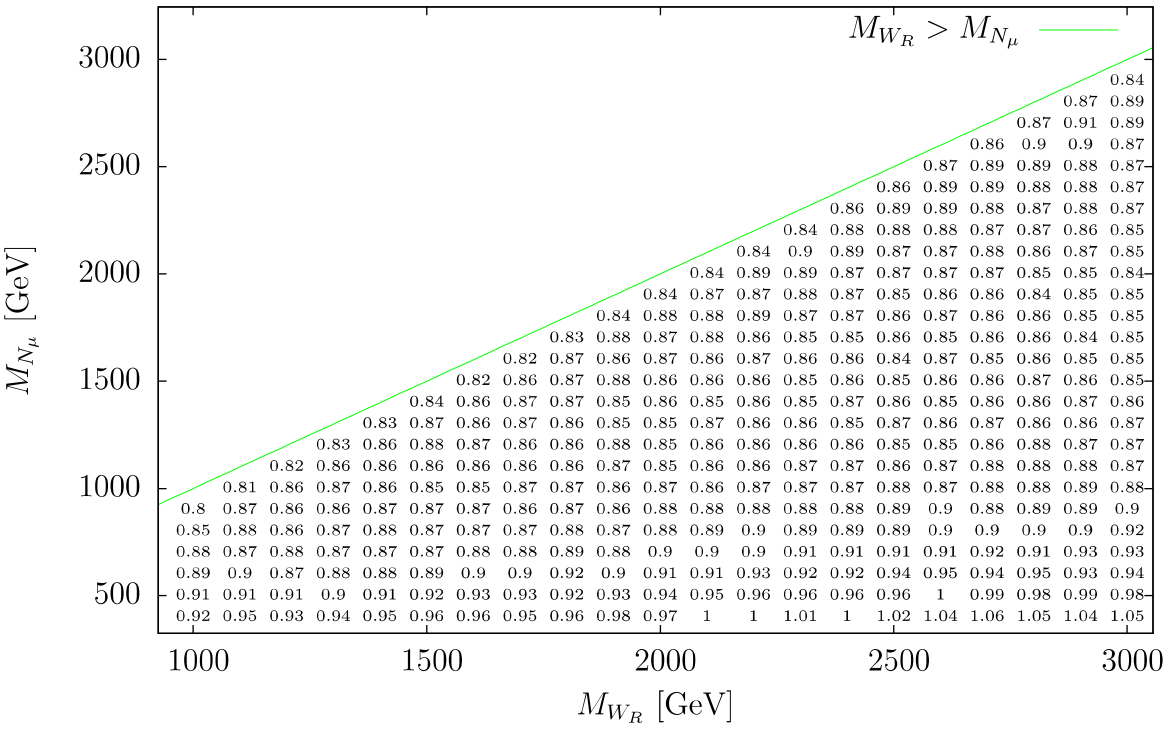

Figure 3.13: Ratio MA5/CMS for muon event acceptance

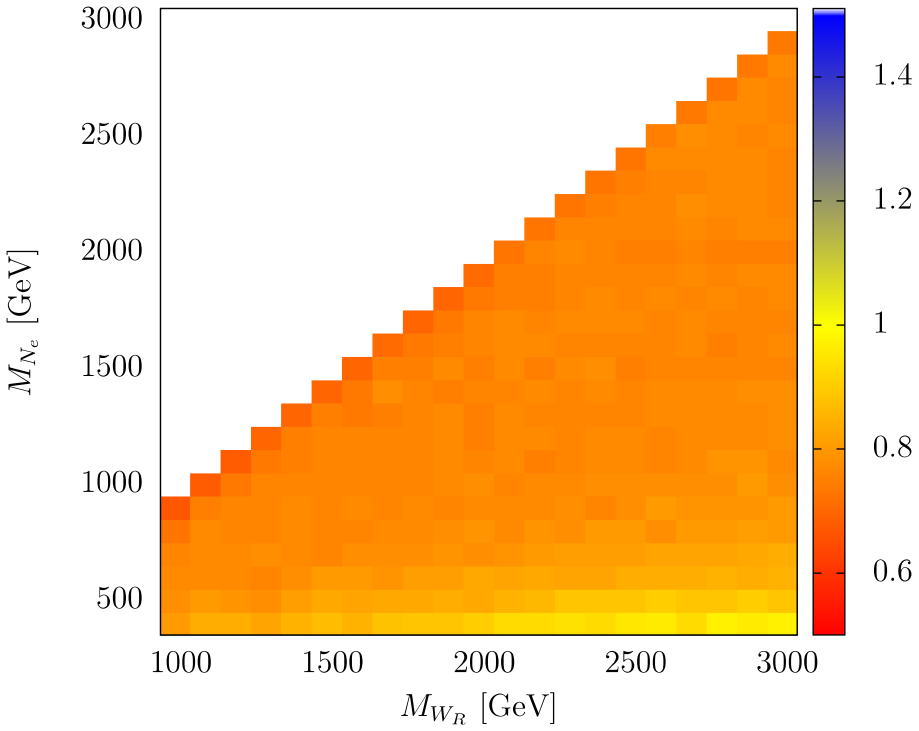

Figure 3.14: Heatmap of the MA5/CMS electron event acceptance ratio

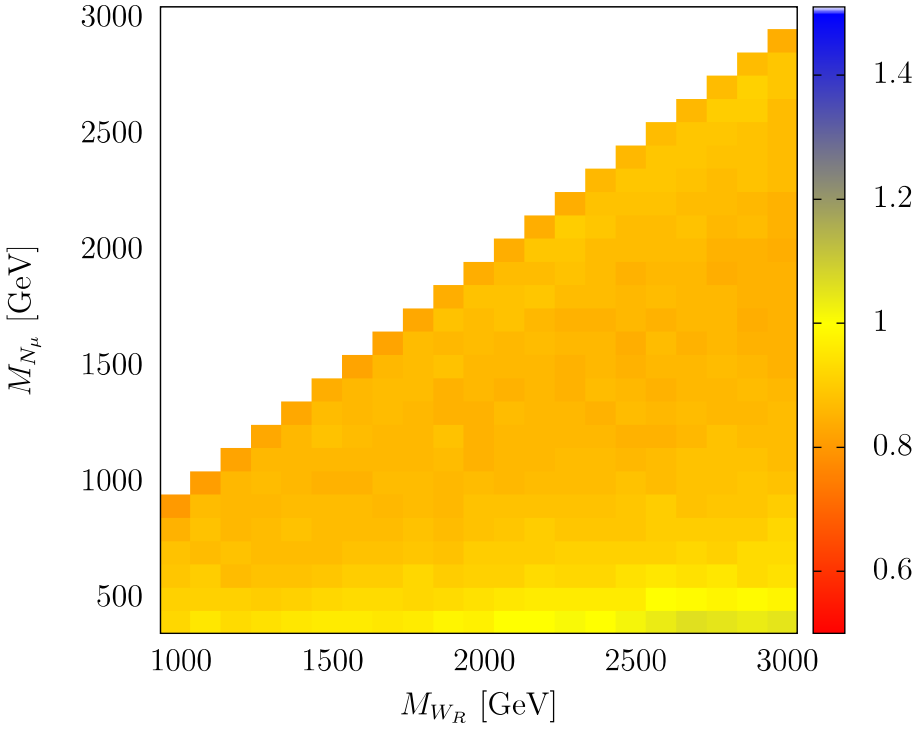

Figure 3.15: Heatmap of the MA5/CMS muon event acceptance ratio

stage	MA5	CMS
selection requirements	28	30
$M_{ee} > 200\,\text{GeV}$	28	29
$M_{eejj} > 600\,\text{GeV}$	28	$29 \pm 1 \pm 3$
selection requirements	31	35
$M_{ee} > 200\,\text{GeV}$	31	35
$M_{\mu\mu jj} > 600\,\text{GeV}$	31	$35 \pm 1 \pm 4$

Table 3.3: Reduction of the simulated event numbers by the two cuts (CMS values from [9] tab.1), the first signal uncertainty of the CMS numbers is the total experimental uncertainty and the second is the PDF uncertainty

The comparison of the muon and electron events shows that the reliability and accuracy of this detector simulation strongly depends on the precision and resolution of the values given in the card. For this reason it is crucial that the needed efficiencies and resolutions were published by the Collaboration of the detector.

6.4 Event numbers

In table 1 of [9] is the number of expected W_R decay events before and after the $M_{ll} > 200\,\text{GeV}$ and $M_{lljj} > 600\,\text{GeV}$ cuts given for $M_{W_R} = 2.5\,\text{TeV}$ and $M_{N_l} = 1.25\,\text{TeV}$. They are compared with the MA5 cut-flow in table 3.3.

The event numbers are always smaller than the CMS numbers, which is expected because of the smaller cross sections and signal acceptance. Nevertheless they are in the total uncertainty range of the CMS values and the number of events before and after the cuts appears to be consistent.

6.5 Exclusion limits

In this section the exclusion limit plots from figure 3 and 5 of [9] are compared with the exclusion limits computed with DelphesMA5tune and MadAnalysis using the MadGraph event files. Figure 3.16 shows the 95% CL excluded area from CMS and MadAnalysis in the M_{W_R}-M_{N_l} plane assuming the first or second neutrino mass scenario. The k-factor was used for all calculations with MadAnalysis.

CMS excludes a larger area for muon events than for electron events. Because of the simpler calculations of exclusion limits, the smaller cross sections and signal acceptance it is not surprising that the 95% CL excluded area in the M_{W_R} M_{N_l} parameter space is much smaller than the excluded area from CMS. Although muon and electron events have a different signal acceptance, the excluded areas for muon and electron events are nearly the same. Thus, the main difference seems to be caused by the smaller cross section or the simplified exclusion limit calculation.

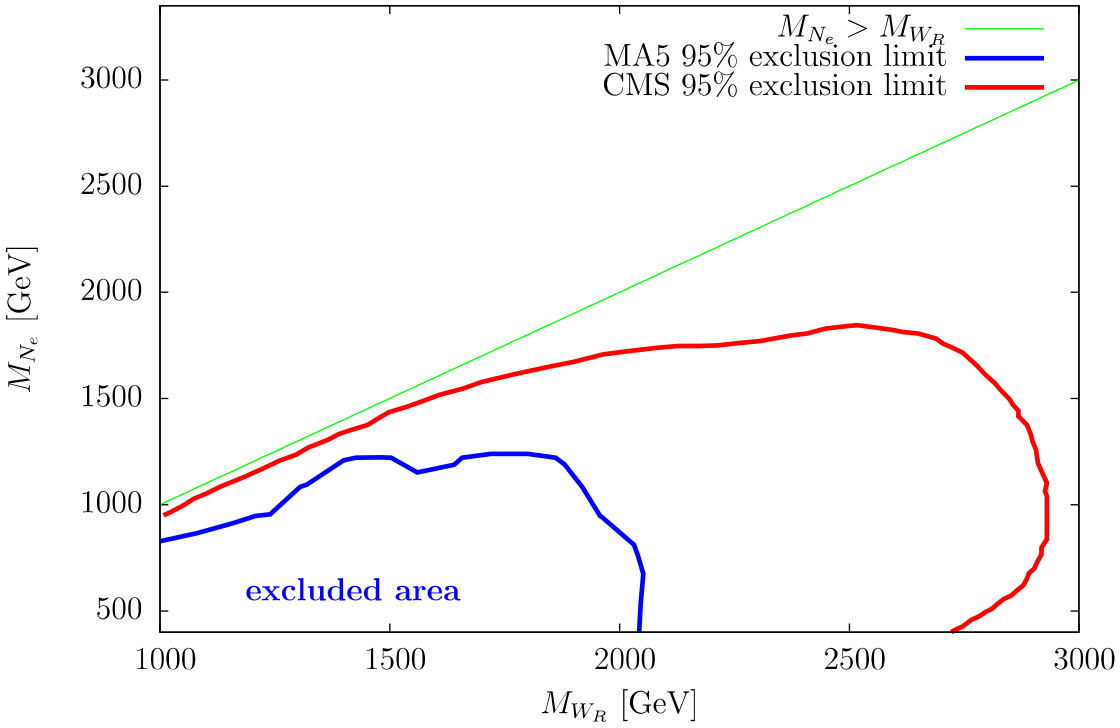

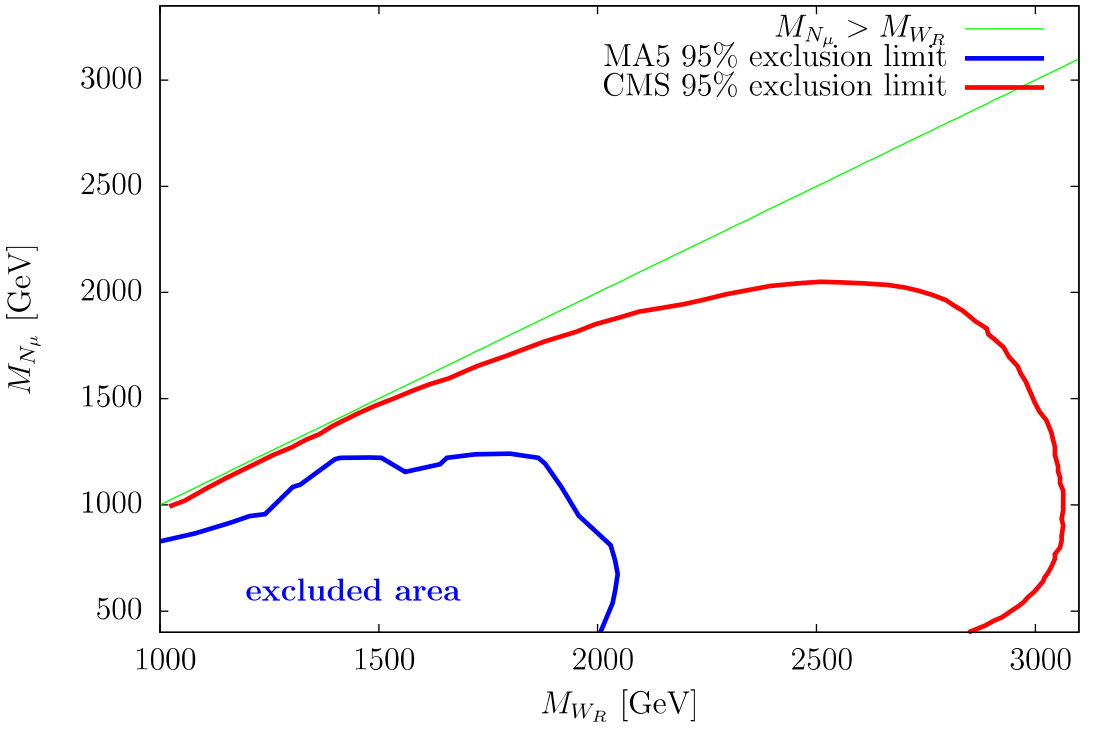

Figure 3.16: Comparison of the electron event (top) and muon event (bottom) 95% exclusion limits from CMS and MA5 assuming $M_{N_{e/\mu}} < M_{W_R} < M_{N_{\mu/e}}, M_{N_\tau}$

To study the influence of the different parts on the deviation, the exclusion limits are computed again with CMS cross sections instead of $\sigma = k \cdot \sigma_{LO}$ or the CMS signal acceptance instead of the fast detector simulation. Figure 3.17(top) shows the the 95% CL excluded area for electron events using the cross section $\sigma = k \cdot k_2 \cdot \sigma_{LO} \approx \sigma_{CMS}$, while 3.17(bottom) shows it with the CMS signal acceptance.

In both cases, the overall influence of the CMS cross sections or the CMS acceptance on the excluded area is rather small, which points on the simpler exclusion limit calculation as the prime cause of the deviation. This is further tested with figure 3.18(top), where the CMS cross sections and the CMS signal acceptance were used at the same time.

The excluded area is very similar to the excluded area with MadGraph cross sections and MA5 signal acceptance as expected from the previous plots. In summary it is very likely, that the largest portion of the deviation is caused by the simpler exclusion limit computation.

Another comparison of exclusion limits for $M_{N_l} = \frac{M_{W_R}}{2}$ is given in figure 3.18(bottom). They show the 95% CL excluded cross sections for $p\ p \to W_R \to e\ e\ j\ j$ calculated with MA5 or by CMS (the excluded cross sections for muon events are in the appendix 6.6).

All 95% CL excluded cross sections are larger than the ones from CMS, which was already expected from the 95% CL excluded area in the mass plane. It was not possible to reproduce the structure of the CMS excluded cross section. This seems to be another limit of either the simpler exclusion limit calculation or the fast detector response simulation.

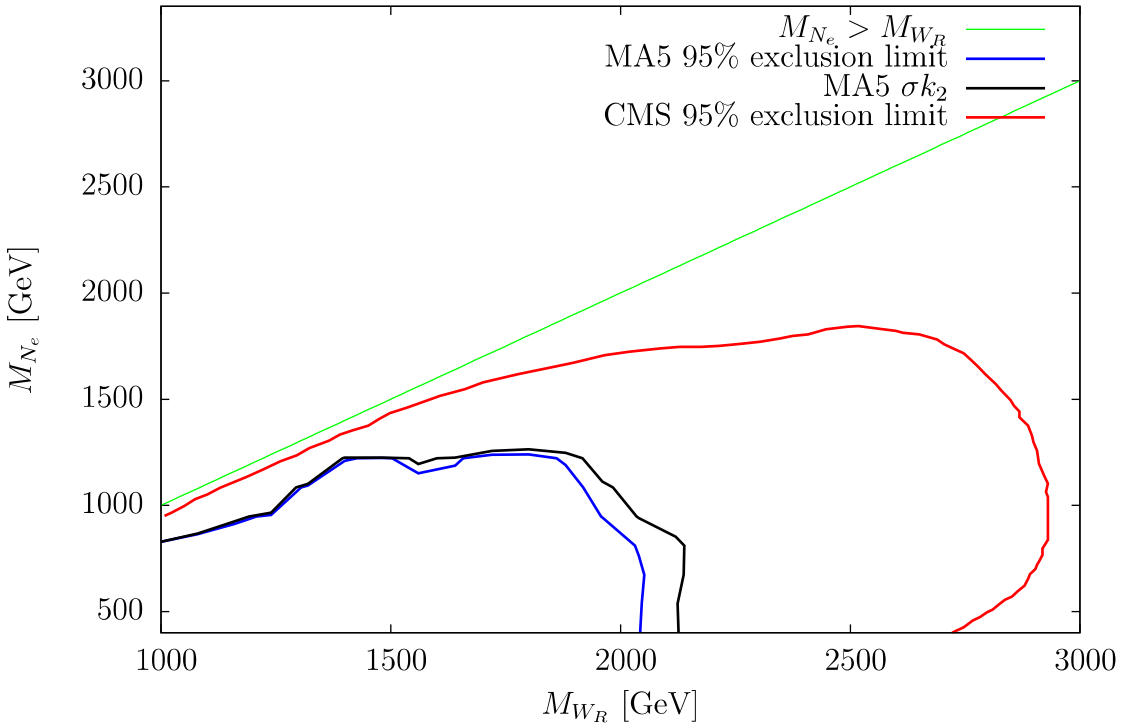

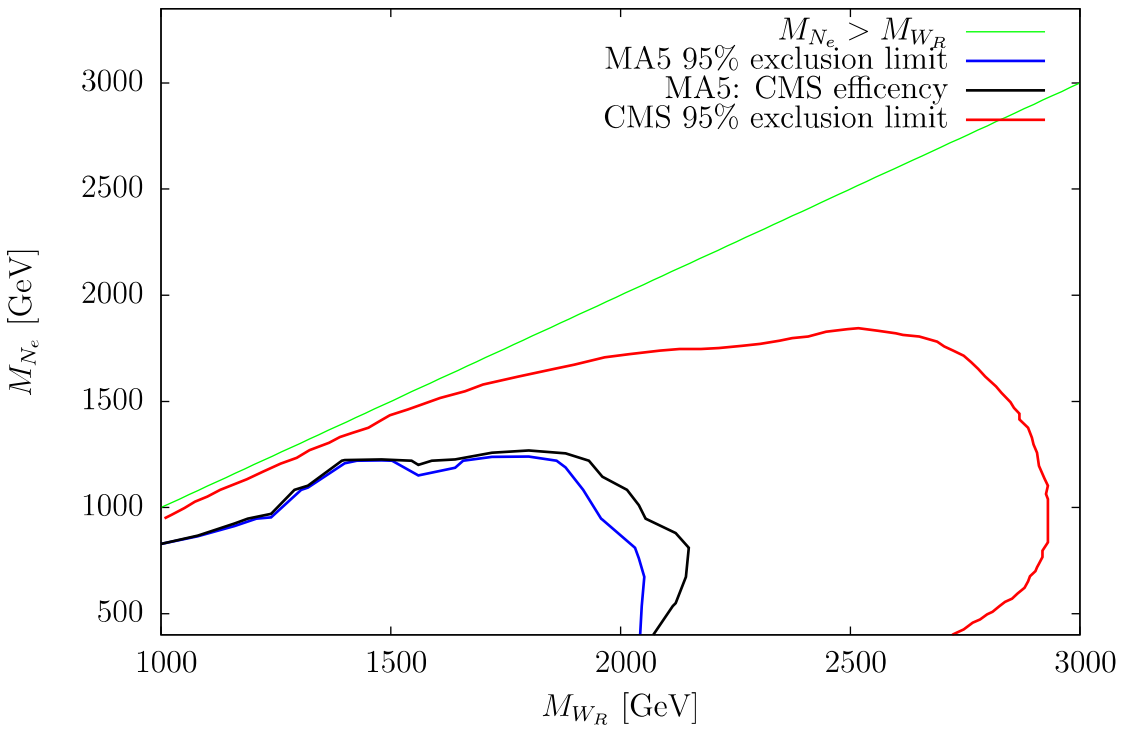

Figure 3.17: Comparison of the electron event 95% exclusion limits from CMS, MA5, MA5 with $\sigma = k \cdot k_2 \cdot \sigma_{LO}$(top) and MA5 with with CMS acceptance(bottom)

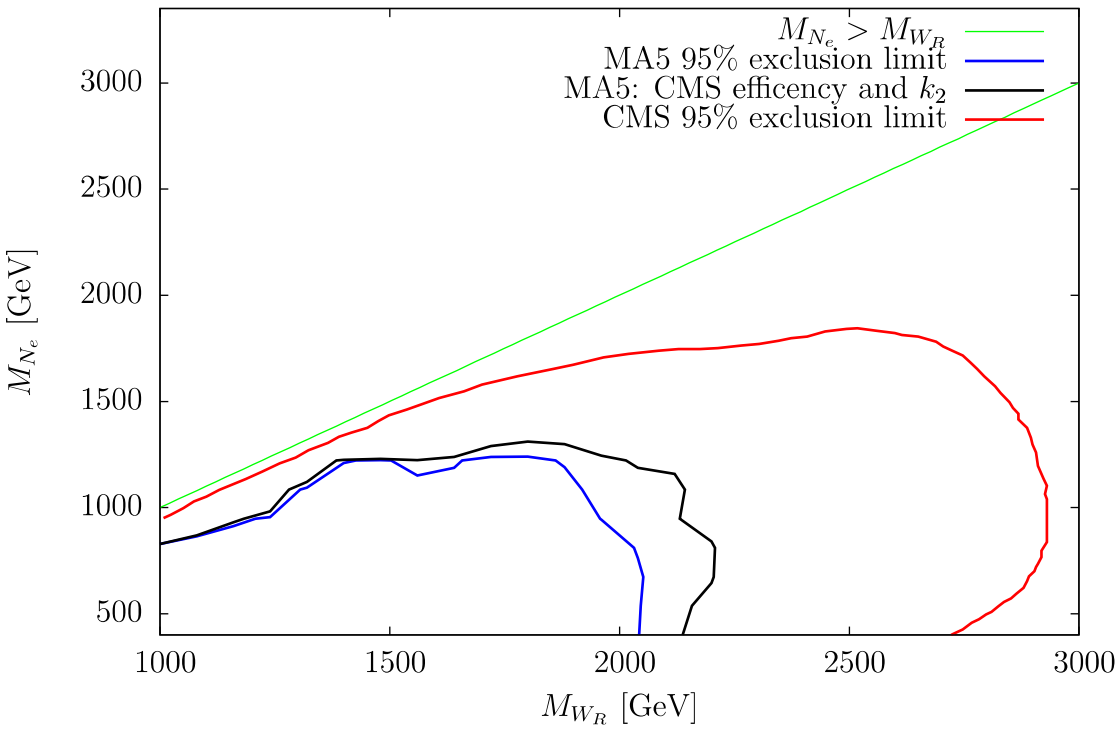

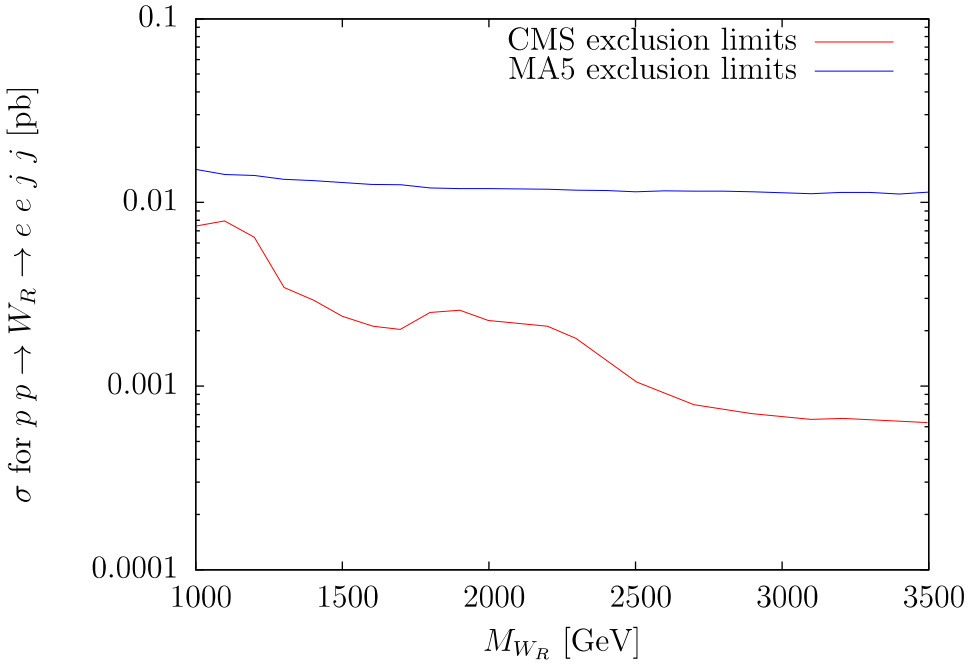

Figure 3.18: Comparison of the electron event 95% exclusion limits from CMS, MA5 and MA5 with CMS acceptance and $\sigma = k \cdot k_2 \cdot \sigma_{LO}(\text{top})$ and Electron event 95% CL excluded $p\ p \to W_R \to eejj$ cross section from CMS and MA5 for $M_{N_e} = \frac{M_{W_R}}{2}$ and $M_{N_e} < M_{W_R} < M_{N_\mu}, M_{N_\tau}$(bottom)

Chapter 4

Application of CMS-EXO-13-008

In the following section we [62] apply the reproduced CMS-EXO-13-008 analysis to the LR-model, which was developed in [20]. In contrast to the model studied in the CMS analysis, strict LR symmetry is not enforced and the mass of the W_R is no longer a free parameter. We use the programs and implementations explained in the previous chapter except for a different model file, which is described in the next section.

1 Implementation in FeynRules

The model file is created according to the parametrization, formulas and the Lagrangian developed in [20], where also their derivation is discussed. Since we are interested in the W_R, we do not use the effective Lagrangian, where it is integrated out, but the fundamental Lagrangian. To speed the event generation and the creation of MadEvent up only the parts of the Lagrangian are implemented, which are necessary for the studied signal. This means we include the kinetic part for fermions, Majorana neutrinos and gauge bosons and the interaction terms between them, while the Higgs sector is completely neglected. We also neglect the mixing between left and right-handed neutrinos and between left and right-handed gauge bosons.

The LR models with Higgs triplets and doublets in the first breaking stage are included in the same model file since they differ only in the mass formulas for the gauge bosons. It is possible to switch between them with the help of the parameter "TripletFlag", which has to be set to one for the triplet model and zero for the doublet model. Other values for this parameter should not be used. As previously mentioned we consider only the triplet model here, because we require the existence of heavy Majorana neutrinos for the analysis.

The first part of the model file is the declaration of the gauge groups and their gauge bosons. Unlike [20] the standard representation with the generators $T^a = \frac{1}{2}\sigma_a$ is used for $SU(2)_R$ instead of the conjugate representation. This choice has no influence on the implemented parts of the Lagrangian and the relevant formulas.

The declaration of gauge bosons is followed the definition of the indices for representations, generations and generators. Next, the definition of all particles are determined, which is split in gauge bosons, fermionic gauge eigenstates and fermionic mass eigenstates. The fermionic part differs only for the neutrinos from the SM.

Subsequently, all parameters which consist of masses, couplings and mixing angles are specified. We use a parametrization similar to [20], where the new physics is parametrized by the cosine of the $U(1)_X$ / $SU(2)_L$ mixing angle $\cos\phi$, the ratio of the two symmetry breaking scales x and the sinus of twice the Higgs beta angle $\sin(2\beta)$.

The last part of the model file is the Lagrangian consisting of the gauge and the fermion part. All parameters and formulas are given in the theory chapter and the model file is shown in the appendix.

2 Scan

In order to study the LR triplet model we scan over the parameters $\cos(\phi)$, $\tan(\beta)$, x and the mass of the right-handed Majorana neutrino M_{N_l}. A first scan which uses the reconstructed CMS analysis is show in 4.1.

It is assumed that only the right-handed electron neutrino N_e is contributing to the decay width of the W_R. Thus, the signal only consists of electron events. We allow $\cos(\phi)$ to vary between 0 and 1, x between 1 and 350 and M_{N_e} between 25 GeV and 2500 GeV. $\tan(\beta) = 10$ is set to 10 in this scan. The CMS-EXO-13-008 analysis is applied to all scan points and the exclusion limits are then projected on the M_{W_R}-M_{N_l} plane by calculating M_{W_R}.

W_R masses can be excluded from $M_{W_R} \approx 75\,\text{GeV}$ up to $M_{W_R} \approx 1350\,\text{GeV}$, while the neutrino masses can be excluded up to $M_{N_e} \approx 700\,\text{GeV}$. We therefore can exclude a smaller area in the mass plane compared to a strict LR symmetric model.

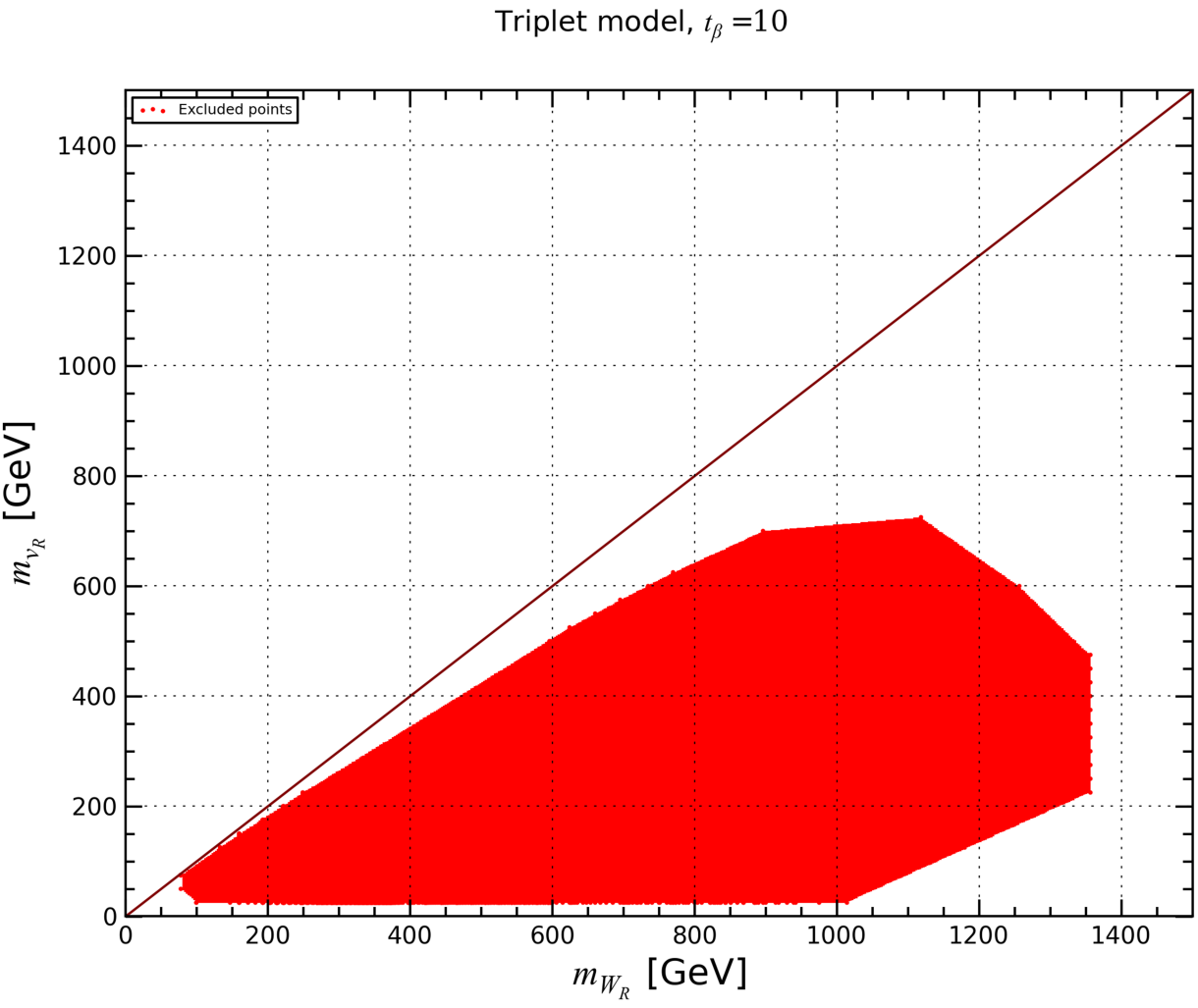

Figure 4.1: 95% excluded area in the M_{W_R}-M_{N_l} plane: $\cos(\phi)$, x and M_{N_l} were varied and the result was projected on the mass plane, $\tan(\beta)$ is fixed to 10

Chapter 5

Conclusion and Outlook

In this work a chain of different programs was used to simulate and analyse the specific signal of the KS process [31]. The different steps were the implementation of the LR model, the event generation, the detector simulation and the event selection. It was possible to reproduce the CMS-EXO-13-008 analysis [9] within the limits of the simulation tools and the published data. A FeynRules [42] LRMSSM model file [19] was cross checked with an independent LR model file and fixed. Another LR model file was created with the Lagrangian and parametrization of [20]. These model files were then used for the event generation. The LO cross section calculated with MadGraph5 was always smaller than the NNLO cross section of CMS and deviations still remained after the usage of a k-factor. On the other hand, the fast detector simulation shows that it is achievable to have an agreement with the full detector simulation below the 20% discrepancy expected for a fast simulation with Delphes. Very important for a good signal acceptance with the same behaviour as the experimental values is the implementation of detailed detector efficiencies. Thus, the success of the fast detector simulation depends on the available data. All cuts and steps necessary for the selection of muon and electron events were implemented in MadAnalysis. They gave reasonable event numbers and reduced them in a similar way as the CMS simulation. Yet, the exclusion limits were much smaller than the CMS exclusion limits. Cross section and signal acceptance were lower than the CMS values, but it turned out that the major effect for the difference is the exclusion limit calculation itself. While the employed script uses a simplified CLs prescription and takes only the total number of events into account, the full CMS analysis is shape based and uses multiple bins of the M_{lljj} distribution. To improve the statistical evaluation more details of the background and the measured event numbers would be needed.

The implementation of the analysis could be used in coming global analyses of the triplet LR model and its supersymmetric extension. It could be combined with electro-weak precision data, the search for doubly charged Higgs bosons or with constraints of processes like dijet or $t\,\bar{t}$ production. Another possibility is to modify the event analysis in order to study similar signals in other models.

1 Danksagung

Ich möchte folgenden Personen danken:

- Prof. Dr. Michael Klasen für die Möglichkeit die Masterarbeit in seiner freundlichen Arbeitsgruppe zu schreiben und die Betreuung
- Prof. Dr. Benjamin Fuks für die gute Zusammenarbeit, die Hilfe während des Projekts und den herzlichen Empfang in Straßburg
- Marcel Rothering für die Hilfe und die Zeit, die er sich genommen hat um mir zu helfen
- David Regalado Lamprea für die erhellenden Diskussionen über Mathematik, Informatik und Physik und für die Hilfe bei allem, was mit Computern zu tun hat
- Forian König dafür, dass er die Skripte zum Laufen bekommen hat
- Saskia Schmiemann für das Korrekturlesen
- meiner Freundin Emely Verweyen für das Korrekturlesen
- der ganze Arbeitsgruppe, ohne die die Arbeitszeit weit weniger unterhaltsam wäre
- Familie, Freunde, Bekannte und Verwandte

Bibliography

[1] S. Chatrchyan *et al.* [CMS Collaboration], "Observation of a new boson at a mass of 125 GeV with the CMS experiment at the LHC," Phys. Lett. B **716** (2012) 30 [arXiv:1207.7235 [hep-ex]].

[2] G. Aad *et al.* [ATLAS Collaboration], "Observation of a new particle in the search for the Standard Model Higgs boson with the ATLAS detector at the LHC," Phys. Lett. B **716** (2013) 1 [arXiv:1207.7214 [hep-ex]].

[3] J. C. Pati and A. Salam, "Lepton Number as the Fourth Color," Phys. Rev. D **10** (1974) 275 [Phys. Rev. D **11** (1975) 703].

[4] R. N. Mohapatra and J. C. Pati, "A Natural Left-Right Symmetry," Phys. Rev. D **11** (1975) 2558.

[5] R. N. Mohapatra and J. C. Pati, "Left-Right Gauge Symmetry and an Isoconjugate Model of CP Violation," Phys. Rev. D **11** (1975) 566.

[6] G. Senjanovic and R. N. Mohapatra, "Exact Left-Right Symmetry and Spontaneous Violation of Parity," Phys. Rev. D **12** (1975) 1502.

[7] G. Senjanovic, "Spontaneous Breakdown of Parity in a Class of Gauge Theories," Nucl. Phys. B **153** (1979) 334.

[8] R. N. Mohapatra and G. Senjanovic, "Neutrino Mass and Spontaneous Parity Violation," Phys. Rev. Lett. **44** (1980) 912.

[9] V. Khachatryan *et al.* [CMS Collaboration], "Search for heavy neutrinos and W bosons with right-handed couplings in proton-proton collisions at $\sqrt{s} = 8\,\text{TeV}$," Eur. Phys. J. C **74** (2014) 11, 3149 [arXiv:1407.3683 [hep-ex]].

[10] S. Chatrchyan *et al.* [CMS Collaboration], "Search for heavy neutrinos and W[R] bosons with right-handed couplings in a left-right symmetric model in pp collisions at sqrt(s) = 7 TeV," Phys. Rev. Lett. **109** (2012) 261802 [arXiv:1210.2402 [hep-ex]].

[11] K.A. Olive et al. (Particle Data Group), "The Review of Particle Physics 2014 Edition", Chin. Phys. C **38** (2014) 090001.

[12] S. Chatrchyan *et al.* [CMS Collaboration], "The CMS experiment at the CERN LHC," JINST **3** (2008) S08004.

[13] M. Böhm, A. Denner, H. Joos, "Gauge Theories of the Strong and Electroweak Interaction" B.G.Teubnder Stuttgart Leibzig Wiesbaden third edition (2001).

[14] J. C. Collins and D. E. Soper, "The Theorems of Perturbative QCD," Ann. Rev. Nucl. Part. Sci. **37** (1987) 383.

[15] T. Sjostrand, S. Mrenna and P. Z. Skands, "PYTHIA 6.4 Physics and Manual," JHEP **0605** (2006) 026 [arXiv: hep-ph/0603175].

[16] J. Alwall *et al.*, "MadGraph/MadEvent v4: The New Web Generation," JHEP **0709** (2007) 028 [arXiv:0706.2334 [hep-ph]].

[17] J. Alwall, M. Herquet, F. Maltoni, O. Mattelaer and T. Stelzer, "MadGraph 5 : Going Beyond," JHEP **1106** (2011) 128 [arXiv:1106.0522 [hep-ph]].

[18] H. F. Jones, "Groups, Representations and Physics", Taylor & Francis Group second edition (1998).

[19] A. Alloul, M. Frank, B. Fuks and M. Rausch de Traubenberg, "Chargino and neutralino production at the Large Hadron Collider in left-right supersymmetric models," JHEP **1310** (2013) 033 [arXiv:1307.5073 [hep-ph]].

[20] K. Hsieh, K. Schmitz, J. H. Yu and C.-P. Yuan, "Global Analysis of General SU(2) x SU(2) x U(1) Models with Precision Data," Phys. Rev. D **82** (2010) 035011 [arXiv:1003.3482 [hep-ph]].

[21] K. S. Babu, B. Dutta and R. N. Mohapatra, "Partial Yukawa unification and a supersymmetric origin of flavor mixing," Phys. Rev. D **60** (1999) 095004 [hep-ph/9812421].

[22] R. Kuchimanchi, "Solution to the strong CP problem: Supersymmetry with parity," Phys. Rev. Lett. **76** (1996) 3486 [hep-ph/9511376].

[23] R. N. Mohapatra and A. Rasin, "A Supersymmetric solution to CP problems," Phys. Rev. D **54** (1996) 5835 [hep-ph/9604445].

[24] R. N. Mohapatra and A. Rasin, "Simple supersymmetric solution to the strong CP problem," Phys. Rev. Lett. **76** (1996) 3490 [hep-ph/9511391].

[25] L. Vale Silva, "Constraining the Doublet Left-Right Model," PoS FWNP (2015) 020 [arXiv:1501.05483 [hep-ph]].

[26] N. G. Deshpande, J. F. Gunion, B. Kayser and F. I. Olness, "Left-right symmetric electroweak models with triplet Higgs," Phys. Rev. D **44** (1991) 837.

[27] B. Dutta, R. Eusebi, Y. Gao, T. Ghosh and T. Kamon, "Exploring the doubly charged Higgs boson of the left-right symmetric model using vector boson fusionlike events at the LHC," Phys. Rev. D **90** (2014) 055015 [arXiv:1404.0685 [hep-ph]].

[28] S. Chatrchyan *et al.* [CMS Collaboration], "A search for a doubly-charged Higgs boson in pp collisions at $\sqrt{s} = 7$ TeV," Eur. Phys. J. C **72** (2012) 2189 [arXiv:1207.2666 [hep-ex]].

[29] G. Bambhaniya, J. Chakrabortty, J. Gluza, T. Jeliński and M. Kordiaczynska, "Lowest limits on the doubly charged Higgs boson masses in the minimal left-right symmetric model," Phys. Rev. D **90** (2014) 9, 095003 [arXiv:1408.0774 [hep-ph]].

[30] M. Nemevsek, F. Nesti, G. Senjanovic and Y. Zhang, "First Limits on Left-Right Symmetry Scale from LHC Data," Phys. Rev. D **83** (2011) 115014 [arXiv:1103.1627 [hep-ph]].

[31] W. Y. Keung and G. Senjanovic, "Majorana Neutrinos and the Production of the Right-handed Charged Gauge Boson," Phys. Rev. Lett. **50** (1983) 1427.

[32] T. Han, I. Lewis, R. Ruiz and Z. g. Si, "Lepton Number Violation and W' Chiral Couplings at the LHC," Phys. Rev. D **87** (2013) 3, 035011 [Phys. Rev. D **87** (2013) 3, 039906] [arXiv:1211.6447 [hep-ph]].

[33] R. Gavin, Y. Li, F. Petriello and S. Quackenbush, "FEWZ 2.0: A code for hadronic Z production at next-to-next-to-leading order," Comput. Phys. Commun. **182** (2011) 2388 [arXiv:1011.3540 [hep-ph]].

[34] J. Botts *et al.* [CTEQ Collaboration], "CTEQ parton distributions and flavor dependence of sea quarks," Phys. Lett. B **304** (1993) 159 [hep-ph/9303255].

[35] R. Field, "Early LHC Underlying Event Data - Findings and Surprises," arXiv:1010.3558 [hep-ph].

[36] S. Agostinelli *et al.* [GEANT4 Collaboration], "GEANT4: A Simulation toolkit," Nucl. Instrum. Meth. A **506** (2003) 250.

[37] C. Degrande, C. Duhr, B. Fuks, D. Grellscheid, O. Mattelaer and T. Reiter, "UFO - The Universal FeynRules Output," Comput. Phys. Commun. **183** (2012) 1201 [arXiv:1108.2040 [hep-ph]].

[38] B. Dumont *et al.*, "Toward a public analysis database for LHC new physics searches using MADANALYSIS 5," Eur. Phys. J. C **75** (2015) 2, 56 [arXiv:1407.3278 [hep-ph]].

[39] E. Conte, B. Fuks and G. Serret, "MadAnalysis 5, A User-Friendly Framework for Collider Phenomenology," Comput. Phys. Commun. **184** (2013) 222 [arXiv:1206.1599 [hep-ph]].

[40] E. Conte and B. Fuks, "MadAnalysis 5: status and new developments," J. Phys. Conf. Ser. **523** (2014) 012032 [arXiv:1309.7831 [hep-ph]].

[41] E. Conte, B. Dumont, B. Fuks and C. Wymant, "Designing and recasting LHC analyses with MadAnalysis 5," Eur. Phys. J. C **74** (2014) 10, 3103 [arXiv:1405.3982 [hep-ph]].

[42] A. Alloul, N. D. Christensen, C. Degrande, C. Duhr and B. Fuks, "FeynRules 2.0 - A complete toolbox for tree-level phenomenology," Comput. Phys. Commun. **185** (2014) 2250 [arXiv:1310.1921 [hep-ph]].

[43] S. Ask *et al.*, "From Lagrangians to Events: Computer Tutorial at the MC4BSM-2012 Workshop," arXiv:1209.0297 [hep-ph].

[44] A. Roitgrund, G. Eilam and S. Bar-Shalom, "Implementation of the left-right symmetric model in FeynRules/CalcHep," arXiv:1401.3345 [hep-ph].

[45] M. R. Whalley, D. Bourilkov and R. C. Group, "The Les Houches accord PDFs (LHAPDF) and LHAGLUE," hep-ph/0508110.

[46] J. de Favereau *et al.* [DELPHES 3 Collaboration], "DELPHES 3, A modular framework for fast simulation of a generic collider experiment," JHEP **1402** (2014) 057 [arXiv:1307.6346 [hep-ex]].

[47] B. Dumont, B. Fuks and C. Wymant, "MadAnalysis 5 implementation of CMS-SUS-13-011: search for stops in the single lepton final state at 8 TeV,"

[48] S. Chatrchyan *et al.* [CMS Collaboration], "Description and performance of track and primary-vertex reconstruction with the CMS tracker," JINST **9** (2014) 10, P10009 [arXiv:1405.6569 [physics.ins-det]].

[49] [CMS Collaboration], "Measurement of Tracking Efficiency," CMS-PAS-TRK-10-002, http://cds.cern.ch/record/1279139/?ln=de.

[50] [CMS Collaboration], "Muon ID and Isolation Efficiencies in 2012 RunAB," CMS-DP-2012-025, http://cms.cern.ch/iCMS/jsp/db_notes/noteInfo.jsp?cmsnoteid=CMS%20DP-2012/025.

[51] [CMS Collaboration], "Electron performance with 19.6 fb^{-1} of data collected at $\sqrt{s} = 8$ TeV with the CMS detector.," CMS-DP-2013-003, http://cds.cern.ch/record/1523273?ln=en.

[52] S. Chatrchyan *et al.* [CMS Collaboration], "Search for Resonances in the Dilepton Mass Distribution in pp Collisions at $\sqrt{(s)} = 7$ TeV," JHEP **1105** (2011) 093 [arXiv:1103.0981 [hep-ex]].

[53] S. Chatrchyan *et al.* [CMS Collaboration], "Search for heavy narrow dilepton resonances in pp collisions at $\sqrt{s} = 7$ TeV and $\sqrt{s} = 8$ TeV," Phys. Lett. B **720** (2013) 63 [arXiv:1212.6175 [hep-ex]].

[54] S. Chatrchyan *et al.* [CMS Collaboration], "Search for leptonic decays of W ' bosons in pp collisions at $\sqrt{s} = 7$ TeV," JHEP **1208** (2012) 023 [arXiv:1204.4764 [hep-ex]].

[55] M. Cacciari, G. P. Salam and G. Soyez, "The Anti-k(t) jet clustering algorithm," JHEP **0804** (2008) 063 [arXiv:0802.1189 [hep-ph]].

[56] M. Cacciari, G. P. Salam and G. Soyez, "FastJet user manual," Eur. Phys. J. C **72** (2012) 1896 [arXiv:1111.6097 [hep-ph]].

[57] M. Cacciari and G. P. Salam, "Dispelling the N^3 myth for the k_t jet-finder," Phys. Lett. B **641** (2006) 57 [hep-ph/0512210].

[58] S. Chatrchyan *et al.* [CMS Collaboration], "Search for narrow resonances in dilepton mass spectra in pp collisions at $\sqrt{s} = 7$ TeV," Phys. Lett. B **714** (2013) 158 [arXiv:1206.1849 [hep-ex]].

[59] T. Junk, "Confidence level computation for combining searches with small statistics," Nucl. Instrum. Meth. A **434** (1999) 435 [hep-ex/9902006].

[60] A. L. Read, "Presentation of search results: The CL(s) technique," J. Phys. G **28** (2002) 2693.

[61] L. Moneta *et al.*, "The RooStats Project," PoS ACAT **2010** (2010) 057 [arXiv:1009.1003 [physics.data-an]].

[62] B. Fuks, M. Klasen and D. Schwartländer, In preparation.

Plagiatserklärung der / des Studierenden

Hiermit versichere ich, dass die vorliegende Arbeit über

_____

_____ selbstständig verfasst worden ist, dass keine anderen Quellen und Hilfsmittel als die angegebenen benutzt worden sind und dass die Stellen der Arbeit, die anderen Werken – auch elektronischen Medien – dem Wortlaut oder Sinn nach entnommen wurden, auf jeden Fall unter Angabe der Quelle als Entlehnung kenntlich gemacht worden sind.

_____

(Datum, Unterschrift)

Ich erkläre mich mit einem Abgleich der Arbeit mit anderen Texten zwecks Auffindung von Übereinstimmungen sowie mit einer zu diesem Zweck vorzunehmenden Speicherung der Arbeit in eine Datenbank einverstanden.

_____

(Datum, Unterschrift)

Chapter 6

Appendix

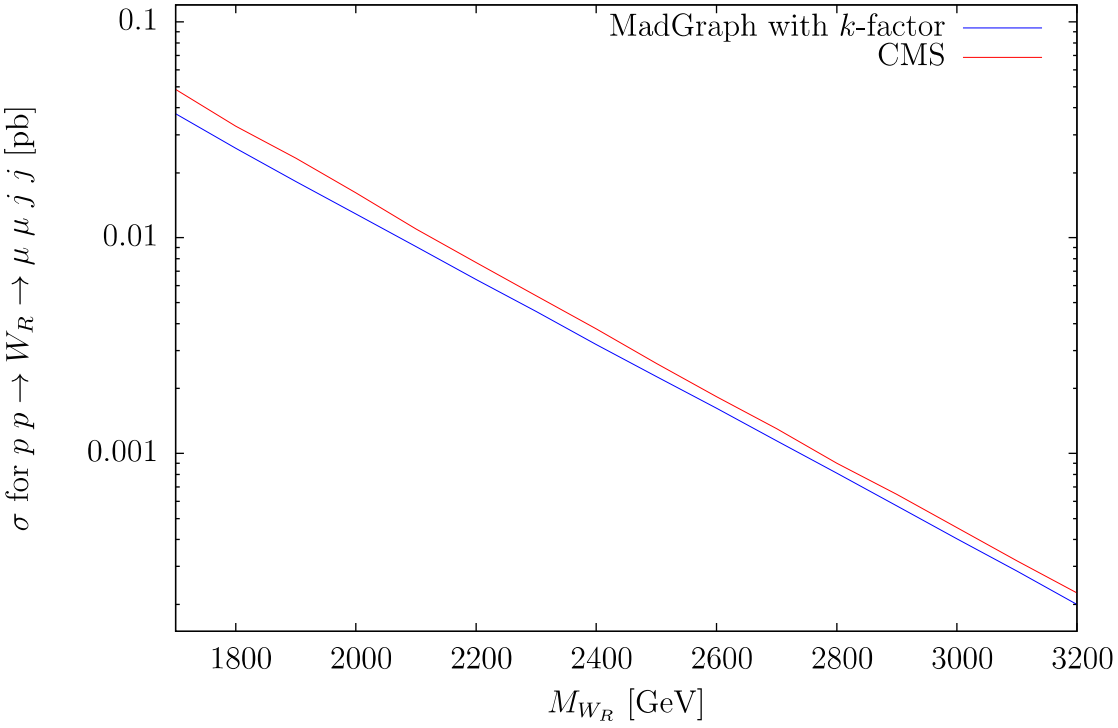

Figure 6.1: Comparison of cross sections for $M_{N_\mu} = \frac{M_{W_R}}{2}$ and $M_{N_\mu} < M_{W_R} < M_{N_e}, M_{N_\tau}$

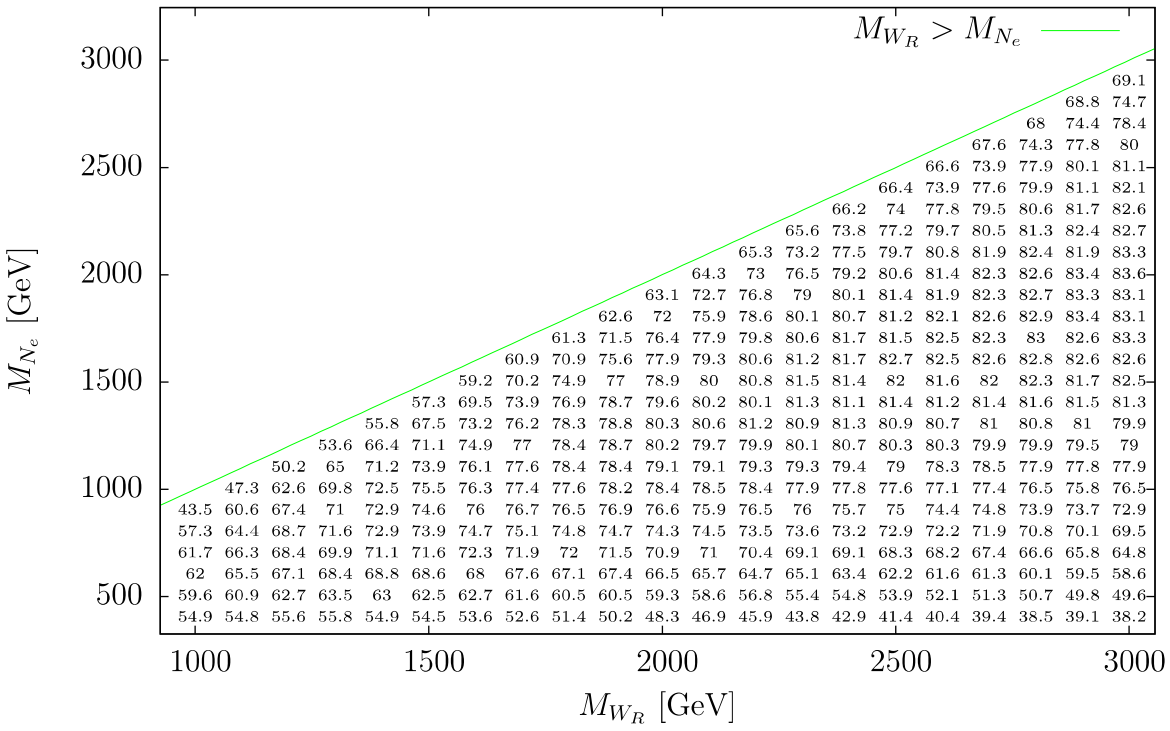

Figure 6.2: CMS signal acceptance for electron events [%]

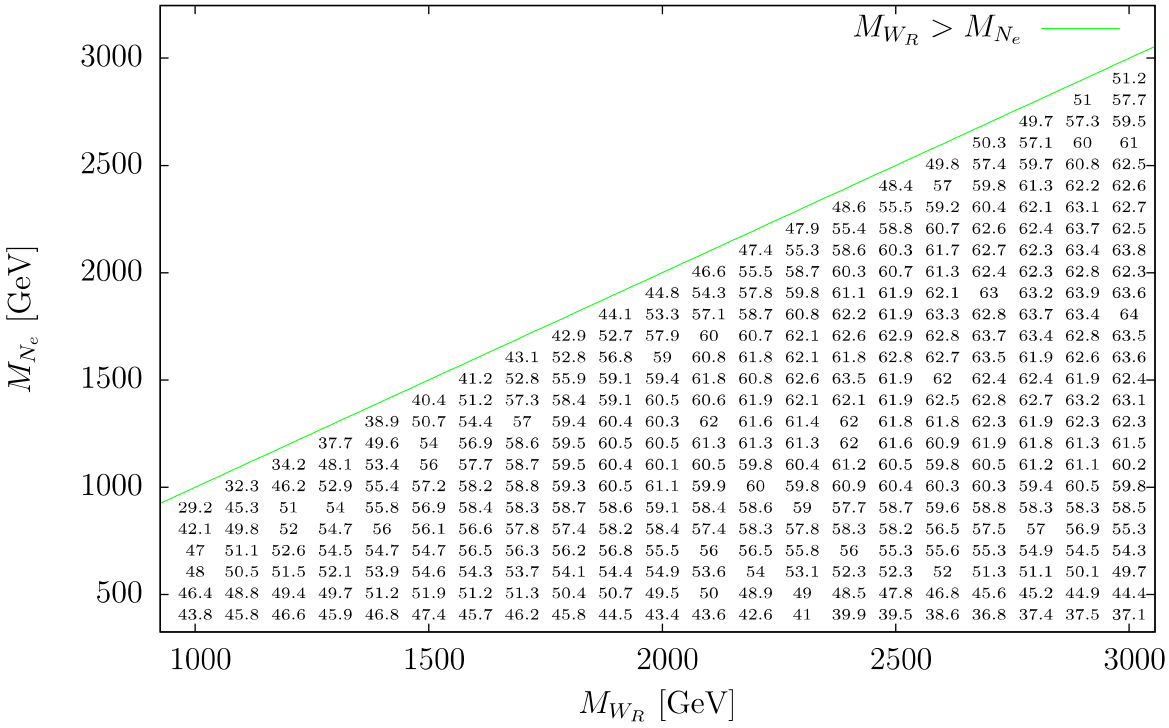

Figure 6.3: Electron event acceptance calculated with DelphesMA5tune [%]

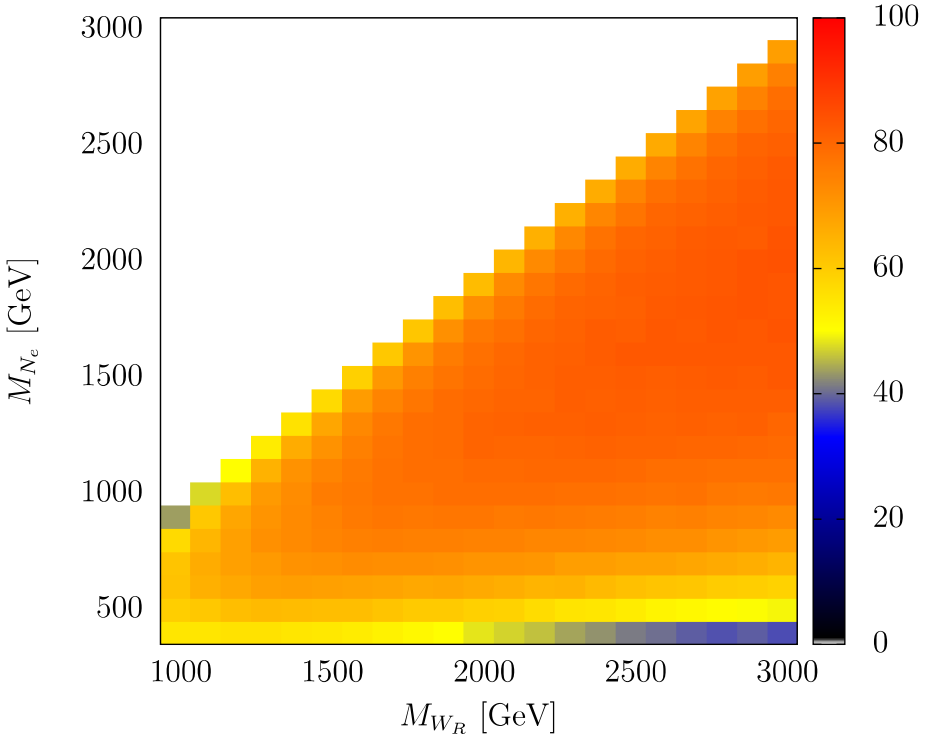

Figure 6.4: Heatmap of CMS electron event acceptance [%]

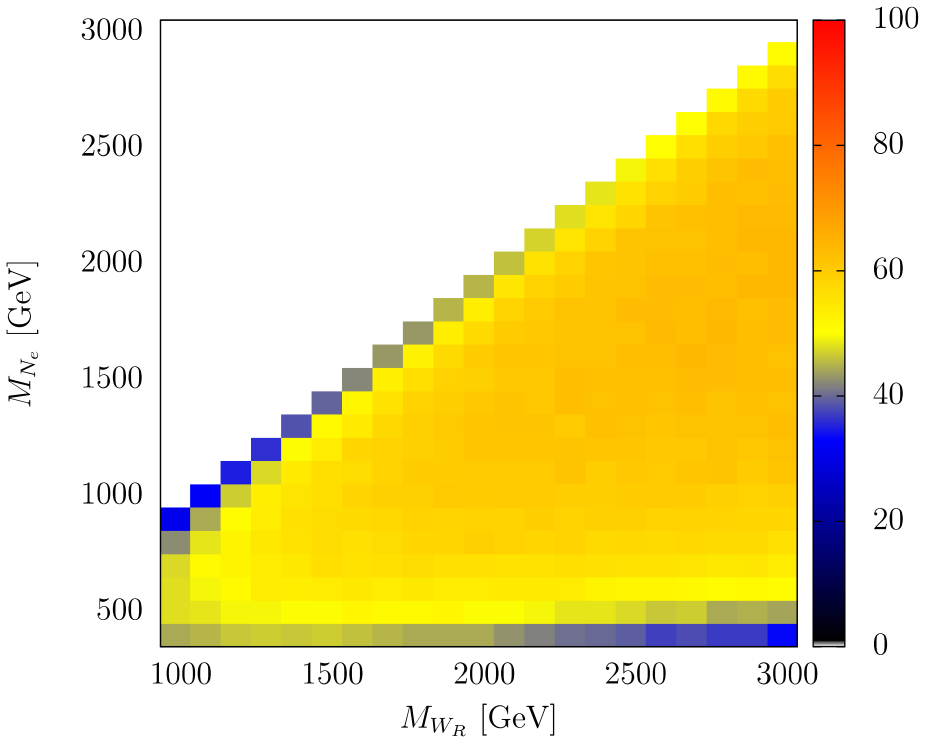

Figure 6.5: Heatmap of MA5 electron event acceptance [%]

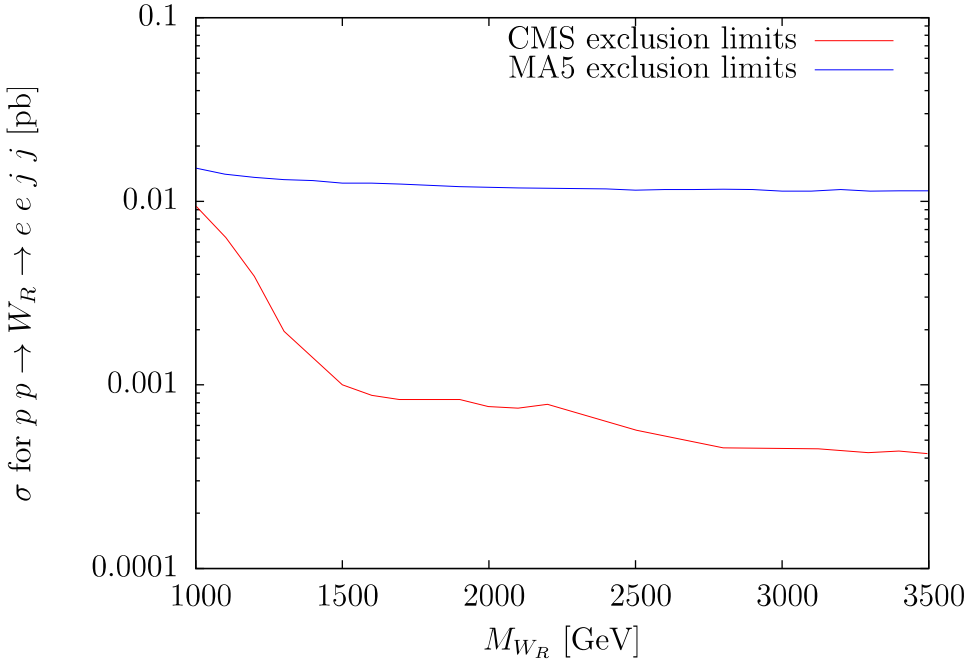

Figure 6.6: Muon event 95% Cl excluded $p\ p \rightarrow W_R \rightarrow \mu\ \mu\ j\ j$ cross section from CMS and MA5 assuming $M_{N_\mu} = \frac{M_{W_R}}{2}$ and $M_{N_\mu} < M_{W_R} < M_{N_e}, M_{N_\tau}$

```
#ifndef analysis_cms_exo_13_008_h
#define analysis_cms_exo_13_008_h

#include "SampleAnalyzer/Process/Analyzer/AnalyzerBase.h"

namespace MA5
{
class cms_exo_13_008 : public AnalyzerBase
{
  INIT_ANALYSIS(cms_exo_13_008,"cms_exo_13_008")

 public:
  virtual bool Initialize(const MA5::Configuration& cfg, const
std::map<std::string,std::string>& parameters);
  virtual void Finalize(const SampleFormat& summary, const
std::vector<SampleFormat>& files);
  virtual bool Execute(SampleFormat& sample, const EventFormat& event);

 template<typename T1, typename T2> void OverlapRemoval(std::vector<const T1*> &
v1, std::vector<const T2*> v2, const double & dr)
 {
 for(int i=v1.size()-1; i>=0; i--)
 for(unsigned int j=0; j<v2.size(); j++)
 if(v1[i]->dr(v2[j])<dr)
 {
 v1.erase(v1.begin()+i);
 break;
 }
 return;
 }

 private:
};
}

#endif
```

```
#include "SampleAnalyzer/User/Analyzer/cms_exo_13_008.h"
using namespace MA5;
using namespace std;

// -----------------------------------------------------------------------------
// Initialize
// function called one time at the beginning of the analysis
// -----------------------------------------------------------------------------
bool cms_exo_13_008::Initialize(const MA5::Configuration& cfg, const
std::map<std::string,std::string>& parameters)
{
  // Information on the analysis, authors, ...
  INFO << "        <><><><><><><><><><><><><><><><><><><><><><><><><><><><><><><><><><>" <<
endmsg;
  INFO << "        <> Analysis: CMS-EXO-13-008 , arXiv:1407.3683v2 <>" <<
endmsg;
  INFO << "        <>         (right-handed neutrinos, WR boson)   <>" <<
endmsg;
  INFO << "        <>  Recasted by: B.Fuks & D.Schwartländer       <>" <<
endmsg;
  INFO << "        <>  Contact: fuks@cern.ch                       <>" <<
endmsg;
  INFO << "        <>           d_schw20@uni-muenster.de           <>" <<
endmsg;
  INFO << "        <>  Based on MadAnalysis 5 v1.1.12              <>" <<
endmsg;
  INFO << "        <>  For more information, see                   <>" <<
endmsg;
  INFO << "        <>
http://madanalysis.irmp.ucl.ac.be/wiki/PhysicsAnalysisDatabase" << endmsg;
  INFO << "        <><><><><><><><><><><><><><><><><><><><><><><><><><><><><><><><><><>" << endmsg;


// initialize the two different regions
  Manager()->AddRegionSelection("2 Jets 2 Electrons");
  Manager()->AddRegionSelection("2 Jets 2 Muons");

// declare all used Cuts and the regions they apply to
  Manager()->AddCut("2 leading Jets");
  Manager()->AddCut("Electron candidates", "2 Jets 2 Electrons");
  Manager()->AddCut("Muon candidates", "2 Jets 2 Muons");
  Manager()->AddCut("Mll > 200GeV");
  Manager()->AddCut("Mlljj > 600GeV");

// declare all histograms
  Manager()->AddHisto("Mee",22,0,500,"2 Jets 2 Electrons"); //fig. 1 a)
  Manager()->AddHisto("Mmumu",22,0,500,"2 Jets 2 Muons"); //fig. 1 b)
  Manager()->AddHisto("Meejj",20,0,4000,"2 Jets 2 Electrons"); //fig. 2 a)
  Manager()->AddHisto("Mmumujj",20,0,4000,"2 Jets 2 Muons"); //fig. 2 b)
  Manager()->AddHisto("Meejj for analysis",20,0,4000,"2 Jets 2 Electrons");
//for confidence intervalls
  Manager()->AddHisto("Mmumujj for analysis",20,0,4000,"2 Jets 2 Muons"); //for
confidence intervalls

  return true;
}

// -----------------------------------------------------------------------------
// Finalize
// function called one time at the end of the analysis
// -----------------------------------------------------------------------------
void cms_exo_13_008::Finalize(const SampleFormat& summary, const
std::vector<SampleFormat>& files)
{
```

```
  // saving histos
}

// ----------------------------------------------------------------------------
// Execute
// function called each time one event is read
// ----------------------------------------------------------------------------
bool cms_exo_13_008::Execute(SampleFormat& sample, const EventFormat& event)
{
 if (event.rec()!=0)
 {
//-----------------------------------------------------------------------------
// set event weight

  double wgt;
  if(Configuration().IsNoEventWeight()) wgt=1.;
  else if(event.mc()->weight()!=0.) wgt=event.mc()->weight();
  else
  {
  WARNING << "Found one event with a zero weight. Skipping..." << endmsg;
  return false;
  }
  Manager()->InitializeForNewEvent(wgt);


//-----------------------------------------------------------------------------
// declare containers
  std::vector<const RecLeptonFormat*> Electrons, Muons, LeadingLeptons;
  std::vector<const RecJetFormat*> Jets, LeadingJets;



//-----------------------------------------------------------------------------
//-----------------------------------------------------------------------------
// Selection criteria
//-----------------------------------------------------------------------------
//-----------------------------------------------------------------------------



//-----------------------------------------------------------------------------
// Jet Selection and Electron Selection
//-----------------------------------------------------------------------------


// collect all Jets with PT>40GeV in a container (candidates for leading Jets)
  for(unsigned int j=0; j<event.rec()->jets().size(); j++)
  {
  const RecJetFormat *CurrentJet = &(event.rec()->jets()[j]);
  double pt = CurrentJet->pt();
  double eta = fabs(CurrentJet->eta());
  if(pt>40. && eta<2.5)
  Jets.push_back(CurrentJet);
  }


// collect all electrons with pT > 40GeV in a container
  for(unsigned int i=0; i<event.rec()->electrons().size(); i++)
  {
  const RecLeptonFormat *CurrentElectron = &(event.rec()->electrons()[i]);
  double pt = CurrentElectron->pt();
  double eta = fabs(CurrentElectron->eta());
  if(pt>40 && eta<2.5)
  Electrons.push_back(CurrentElectron);
```

```
  }

//------------------------------------------------------------------------------
---
// remove double-counting of electrons as jets by removing the electrons from
the jet container

// Remove them from the jet collection (OverlapRemoval is defined in the header
file)
  OverlapRemoval(Jets,Electrons, 0.2);

// sort the Jets by PT
  SORTER->sort(Jets);

// apply Cut: there are at least two Jets with pT > 40GeV
  if (!Manager()->ApplyCut(Jets.size()>=2,"2 leading Jets")) return true;

// the 2 jets with the highest pT are called leading Jets and they are the only
relevant Jets for the following Analysis
  LeadingJets.push_back(Jets[0]);
  LeadingJets.push_back(Jets[1]);


//------------------------------------------------------------------------------
// isolation criteria for Electrons
//------------------------------------------------------------------------------

// all non-isolated electrons are removed, non-isolated electrons are within a
cone of deltaR < 0.5 around a leading Jet

// Remove the non-isolated electrons with respect to the two leading jets
  OverlapRemoval(Electrons,LeadingJets, 0.5);

// sort electrons by pT
  SORTER->sort(Electrons);


//------------------------------------------------------------------------------
// Muon Selection and isolation criteria
//------------------------------------------------------------------------------

// collect all Muons with pT > 40GeV in a container
  for(unsigned int i=0; i<event.rec()->muons().size(); i++)
  {
  const RecLeptonFormat *CurrentMuon = &(event.rec()->muons()[i]);
  double pt = CurrentMuon->pt();
  double eta = fabs(CurrentMuon->eta());
  if(pt>40 && eta<2.4)
  Muons.push_back(CurrentMuon);
  }

// remove all Muons that are not isolated from Jets (see electron selection)
  OverlapRemoval(Muons,LeadingJets, 0.5);

// sort Muons by pT
  SORTER->sort(Muons);

//------------------------------------------------------------------------------
-
// Second isolation criterium for mouns


// reduction of muons from decay-in-flight: erase every muon if the pT sum of
every track within a cone of deltaR < 0.3 around the muon is larger than 10% of
```

```
the muon pT
  for(int i = Muons.size()-1; i >= 0; i--)
  {
   for(unsigned int j = 0; j < Muons[i]->isolCones().size(); j++)
   {
    if(fabs(Muons[i]->isolCones()[j].deltaR() - 0.3) < 0.001)
     {
      if(Muons[i]->isolCones()[j].sumPT() > 0.10*Muons[i]->pt())
      {
       Muons.erase(Muons.begin()+i);
       break;
      }
     }
   }
  }


//------------------------------------------------------------------------------
// Identifying the Signal-Leptons:
//------------------------------------------------------------------------------


// the lepton with highest pT is called leading lepton while the lepton of the
same-flavour and the second highest pT (of the leptons with the same flavour) is
called subleading lepton

  bool isEE = false, isMUMU=false;

// looking for events that fullfill the requirements for an electron event

// Checking if there are more than two electrons with pT>40GeV and at least one
electron has pT>60GeV
  if(Electrons.size()>=2)
  {
   if(Electrons[0]->pt()>60.) isEE=true;//now the leading/subleading electron is
the frist/second electron in the container
  }


// looking for events that fullfill the requirements for an muon event

// Checking if there are more than two muons with pT>40GeV and at least one muon
has pT>60GeV, one muon must have eta<2.1 to activate the trigger
  int z=1;
  if(Muons.size()>=2)
  {
   if(Muons[0]->pt()>60.)
   {
    if(fabs(Muons[0]->eta())<2.1) isMUMU=true; //now the leading/subleading muon
is the frist/second muon in the container
    else
    {
     for(unsigned int i=1; i<Muons.size(); i++)
     {
      if(fabs(Muons[i]->eta())<2.1)
      {
       isMUMU=true;
       z=i;
       break; //now the leading/subleading muon is the frist/i muon in the
container
      }
     }
    }
   }
```

```
  }

//decide: muon or electron event
  if(isMUMU && isEE)
  {
   if((Muons[0]->pt()+Muons[z]->pt())<(Electrons[0]->pt()+Electrons[1]->pt()))
isMUMU=false;
   else isEE=false;
  }

// apply the cuts (events are put now in one of two regions: electron and muon
event candidates)
  if (!Manager()->ApplyCut(isEE,"Electron candidates")) return true;
  if (!Manager()->ApplyCut(isMUMU,"Muon candidates")) return true;

// trigger efficiency: event-weigth multiplied with the propability that the
event activates the trigger
  if(isEE) Manager()->SetCurrentEventWeight(wgt*.99);
  if(isMUMU) Manager()->SetCurrentEventWeight(wgt*.98);

// Signal lepton collection in container
  if(isEE) { LeadingLeptons.push_back(Electrons[0]);
LeadingLeptons.push_back(Electrons[1]); }
  else { LeadingLeptons.push_back(Muons[0]); LeadingLeptons.push_back(Muons[z]);
}



//-----------------------------------------------------------------------------
//-----------------------------------------------------------------------------
// Cuts to reduce SM-background
//-----------------------------------------------------------------------------
//-----------------------------------------------------------------------------



//-----------------------------------------------------------------------------
// Calculation of Mee, Mmumu, Meejj and Mmumujj
//-----------------------------------------------------------------------------

  double Mll = 0.;
  double Mlljj = 0.;

// calculate M_ll for the two leading Leptons
  TLorentzVector pll;
  for(int e = 0; e < 2; e++)
  {
   TLorentzVector tmp = LeadingLeptons[e]->momentum();
   pll = pll + tmp;
  }
  Mll = pll.M();

// calculate M_lljj for the two leading Jets
  for(int j = 0; j < 2; j++)
  {
   TLorentzVector tmp = Jets[j]->momentum();
   pll = pll + tmp;
  }
  Mlljj = pll.M();



//-----------------------------------------------------------------------------
// Cuts: Mee or Mmumu > 200GeV; Meejj or Mmumujj > 600GeV
```

```
//--------------------------------------------------------------------------

// Mll Cut

// fill histogram
  if(isEE) {Manager()->FillHisto("Mee", Mll);}

// fill histogram
  if(isMUMU) {Manager()->FillHisto("Mmumu", Mll);}

// apply cut Mll > 200.
  if (!Manager()->ApplyCut(Mll > 200.,"Mll > 200GeV")) return true;


//Mlljj Cut

// fill histogram
  if(isEE) {Manager()->FillHisto("Meejj", Mlljj);}

// fill histogram
  if(isMUMU) {Manager()->FillHisto("Mmumujj", Mlljj);}

// apply cut M_lljj > 600GeV
  if (!Manager()->ApplyCut(Mlljj > 600.,"Mlljj > 600GeV")) return true;

// fill histogram
  if(isEE) {Manager()->FillHisto("Meejj for analysis", Mlljj);}

// fill histogram
  if(isMUMU) {Manager()->FillHisto("Mmumujj for analysis", Mlljj);}

}
  return true;
}
```

```
(*************************************************************************
*************************)
(******     FeynRules model file for a simplified G(221)-inspired wprime model
******)
(******     WARNING: the Higgs sector has not been implemented
******)
(******     Authors: B. Fuks
******)
(******
******)
(*************************************************************************
*************************)

(* ************************ *)
(* *****  Information   ***** *)
(* ************************ *)
M$ModelName = "wprime-LR";

M$Information = {
  Authors      -> {"B. Fuks"},
  Version      -> "1.1",
  Date         -> "15. 07. 2015",
  Institutions -> {"IPHC Strasbourg / University of Strasbourg"},
  Emails       -> {"benjamin.fuks@cnrs.in2p3.fr"},
  URLs         -> ""
};

FeynmanGauge = False;

(* ************************ *)
(* *****  Gauge groups  ***** *)
(* ************************ *)
M$GaugeGroups = {
 U1X  == { Abelian -> True,  CouplingConstant -> gX, GaugeBoson -> BX, Charge->X
},
 SU21 == { Abelian -> False, CouplingConstant -> g1,  GaugeBoson -> W1i,
StructureConstant -> ep1, Representations -> {T1,SU2D1},
   Definitions -> {T1[Index[SU2W1,a_],b__]->PauliSigma[Index[SU2W1,a],b]/2, ep1-
>Eps} },
 SU22 == { Abelian -> False, CouplingConstant -> g2,  GaugeBoson -> W2i,
StructureConstant -> ep2, Representations -> {T2,SU2D2},
   Definitions -> {T2[Index[SU2W2,a_],i_,j_]->-PauliSigma[Index[SU2W2,a],j,i]/2,
ep2->Eps} },
 SU3C == { Abelian -> False, CouplingConstant -> gs,  GaugeBoson -> G,
StructureConstant -> f, SymmetricTensor -> dSUN,Representations->{{T,Colour},
{Tb,Colourb}}  }
};

(* ************************ *)
(* *****    Indices     ***** *)
(* ************************ *)
(* Gauge indices *)
IndexRange[Index[SU2W1]]   = Unfold[Range[3]];   IndexStyle[SU2W1,j];
IndexRange[Index[SU2W2]]   = Unfold[Range[3]];   IndexStyle[SU2W2,j];
IndexRange[Index[SU2D1]]   = Unfold[Range[2]];   IndexStyle[SU2D1,k];
IndexRange[Index[SU2D2]]   = Unfold[Range[2]];   IndexStyle[SU2D2,k];
IndexRange[Index[Gluon ]]  = NoUnfold[Range[8]]; IndexStyle[Gluon, a];
IndexRange[Index[Colour ]] = NoUnfold[Range[3]]; IndexStyle[Colour, m];

(* Generation indices *)
IndexRange[Index[GEN ]] = Range[3]; IndexStyle[GEN, f];

(* ************************ *)
(* *** Interaction orders *** *)
```

```
(* ***  (as used by mg5)  *** *)
(* ************************ *)
M$InteractionOrderHierarchy = { {QCD, 1}, {QED, 2} };

(* ************************ *)
(* **** Particle classes **** *)
(* ************************ *)
M$ClassesDescription = {
(* SU(2) triplets and U(1) *)
 V[11] == { ClassName->BX,  Unphysical->True, SelfConjugate->True,
     Definitions -> { BX[mu_] -> cphi (-sth Z[mu]+cth A[mu]) - sphi Zp[mu] } },
 V[12] == { ClassName->W1i, Unphysical->True, SelfConjugate->True, Indices-
>{Index[SU2W1]}, FlavorIndex->SU2W1,
     Definitions -> { W1i[mu_,1] -> (Wbar[mu]+W[mu])/Sqrt[2],   W1i[mu_,2] ->
(Wbar[mu]-W[mu])/(I*Sqrt[2]),   W1i[mu_,3] -> cth Z[mu] + sth A[mu]} },
 V[13] == { ClassName->W2i, Unphysical->True, SelfConjugate->True, Indices-
>{Index[SU2W2]}, FlavorIndex->SU2W2,
     Definitions -> { W2i[mu_,1] -> (Wpbar[mu]+Wp[mu])/Sqrt[2], W2i[mu_,2] ->
(Wpbar[mu]-Wp[mu])/(I*Sqrt[2]), W2i[mu_,3] -> sphi (-sth Z[mu]+cth A[mu]) + cphi
Zp[mu]} },
(* Neutral weak bosons *)
 V[1] == { ClassName->A,  SelfConjugate->True,  Mass->0,              Width->0,
      ParticleName->"a",   PDG->22, PropagatorLabel->"A",  PropagatorType->Sine,
PropagatorArrow->None},
 V[2] == { ClassName->Z,  SelfConjugate->True,  Mass->{MZ, 91.1876},  Width-
>{WZ,2.4952},
      ParticleName->"Z",   PDG->23, PropagatorLabel->"Z",  PropagatorType->Sine,
PropagatorArrow->None},
 V[3] == { ClassName->Zp, SelfConjugate->True,  Mass->{MZp,Internal}, Width-
>{WZp,10.},
      ParticleName->"Zp",  PDG->32, PropagatorLabel->"Zp", PropagatorType->Sine,
PropagatorArrow->None},
(* Charge weak bosons *)
 V[4] == { ClassName->W,  SelfConjugate->False, Mass->{MW, Internal}, Width-
>{WW, 2.085},
      ParticleName->"W+",  PDG->24, PropagatorLabel->"W",  PropagatorType->Sine,
PropagatorArrow->Forward, AntiParticleName->"W-",  QuantumNumbers->{Q->1} },
 V[5] == { ClassName->Wp, SelfConjugate->False, Mass->{MWp,Internal},
Width->{WWp,10.},
      ParticleName->"Wp+", PDG->34, PropagatorLabel->"Wp", PropagatorType->Sine,
PropagatorArrow->Forward, AntiParticleName->"Wp-", QuantumNumbers->{Q->1} },
(* QCD *)
 V[6] == { ClassName->G,  SelfConjugate->True,  Mass->0,              Width->0,
      ParticleName->"g",   PDG->21, PropagatorLabel->"G", PropagatorType->C,
PropagatorArrow->None, Indices->{Index[Gluon]} },

(* Fermionic gauge eigenstates *)
 W[31] == { ClassName->LLw, Unphysical->True, Chirality->Left, SelfConjugate-
>False,
            Indices->{Index[SU2D1],Index[GEN]}, FlavorIndex->SU2D1,
QuantumNumbers->{X ->-1/2},
            Definitions->{LLw[s_,1,ff_]->vLw[s,ff], LLw[s_,2,ff_]->eLw[s,ff]}},
 W[32] == { ClassName->LRw, Unphysical->True, Chirality->Left, SelfConjugate-
>False,
            Indices->{Index[SU2D2],Index[GEN]}, FlavorIndex->SU2D2,
QuantumNumbers->{X -> 1/2},
            Definitions->{LRw[s_,1,ff_]->VRw[s,ff], LRw[s_,2,ff_]->ERw[s,ff]}},
 W[33] == { ClassName->QLw, Unphysical->True, Chirality->Left, SelfConjugate-
>False,
            Indices->{Index[SU2D1],Index[GEN],Index[Colour]},FlavorIndex->SU2D1,
QuantumNumbers->{X -> 1/6},
            Definitions->{QLw[s_,1,ff_,cc_]->uLw[s,ff,cc],
QLw[s_,2,ff_,cc_]:>Module[{ff2}, CKM[ff,ff2] dLw[s,ff2,cc]]}},
 W[34] == { ClassName->QRw, Unphysical->True, Chirality->Left, SelfConjugate-
```

```
>False,
            Indices->{Index[SU2D2],Index[GEN],Index[Colourb]},FlavorIndex-
>SU2D2, QuantumNumbers->{X -> -1/6},
            Definitions->{QRw[s_,1,ff_,cc_]->URw[s,ff,cc],
QRw[s_,2,ff_,cc_]:>Module[{ff2}, CKM[ff,ff2] DRw[s,ff2,cc]]}},
 W[7] == { ClassName->vLw, Unphysical->True, Chirality->Left, SelfConjugate-
>False, Indices->{Index[GEN]}, FlavorIndex->GEN },
 W[8] == { ClassName->eLw, Unphysical->True, Chirality->Left, SelfConjugate-
>False, Indices->{Index[GEN]}, FlavorIndex->GEN },
 W[9] == { ClassName->VRw, Unphysical->True, Chirality->Left, SelfConjugate-
>False, Indices->{Index[GEN]}, FlavorIndex->GEN },
 W[10]== { ClassName->ERw, Unphysical->True, Chirality->Left, SelfConjugate-
>False, Indices->{Index[GEN]}, FlavorIndex->GEN },
 W[11]== { ClassName->uLw, Unphysical->True, Chirality->Left, SelfConjugate-
>False, Indices->{Index[GEN],Index[Colour]},  FlavorIndex->GEN },
 W[12]== { ClassName->dLw, Unphysical->True, Chirality->Left, SelfConjugate-
>False, Indices->{Index[GEN],Index[Colour]},  FlavorIndex->GEN },
 W[13]== { ClassName->URw, Unphysical->True, Chirality->Left, SelfConjugate-
>False, Indices->{Index[GEN],Index[Colourb]}, FlavorIndex->GEN },
 W[14]== { ClassName->DRw, Unphysical->True, Chirality->Left, SelfConjugate-
>False, Indices->{Index[GEN],Index[Colourb]}, FlavorIndex->GEN },
 W[101]== { ClassName->NLw, Unphysical->True, Chirality->Left, SelfConjugate-
>False, Indices->{Index[GEN]}, FlavorIndex->GEN },
 W[102]== { ClassName->NRw, Unphysical->True, Chirality->Left, SelfConjugate-
>False, Indices->{Index[GEN]}, FlavorIndex->GEN },

(* Fermionic mass eigenstates *)
 F[5] == { ClassName->vl, SelfConjugate->True, Indices->{Index[GEN]},
FlavorIndex->GEN, WeylComponents->{vLw,NRwbar},
      ParticleName->{"ve","vm","vt"}, ClassMembers->{ve,vm,vt},
      Mass->0, Width->0, PDG->{12,14,16},
      PropagatorLabel->{"v","ve","vm","vt"},  PropagatorType->Straight,
PropagatorArrow->Forward},
 F[6] == { ClassName->Nl, SelfConjugate->True, Indices->{Index[GEN]},
FlavorIndex->GEN, WeylComponents->{NLw,VRwbar},
      ParticleName->{"Ne","Nm","Nt"}, ClassMembers->{Ne,Nm,Nt},
      Mass->{MNl,{MNe,6000},{MNm,6000},{MNt,6000}}, Width->{WNl,{WNe,10},
{WNm,10},{WNt,10}}, PDG->{6000012,6000014,6000016},
      PropagatorLabel->{"Nl","Ne","Nm","Nt"}, PropagatorType->Straight,
PropagatorArrow->Forward},
 F[7] == { ClassName->l, SelfConjugate->False, Indices->{Index[GEN]},
FlavorIndex->GEN, QuantumNumbers->{Q->-1}, WeylComponents->{eLw,ERwbar},
      ParticleName->{"e-","mu-","tau-"}, AntiParticleName->{"e+","mu+","tau+"},
ClassMembers->{e,m,ta},
      Mass->{Ml, {Me,5.11*^-4}, {MMU,0.10566}, {MTA,1.777}}, Width->0, PDG-
>{11,13,15},
      PropagatorLabel->{"l","e","mu","tau"},  PropagatorType->Straight,
PropagatorArrow->Forward},
 F[8] == { ClassName->uq, SelfConjugate->False, Indices-
>{Index[GEN],Index[Colour]}, FlavorIndex->GEN, QuantumNumbers->{Q-> 2/3},
WeylComponents->{uLw,URwbar},
      ParticleName->{"u","c","t"}, AntiParticleName->{"u~","c~","t~"},
ClassMembers->{u,c,t},
      Mass->{Muq, {MU, 2.55*^-3}, {MC,1.27}, {MT,172}}, Width->{0,0,
{WT,1.50833649}}, PDG->{2,4,6},
      PropagatorLabel->{"uq","u","c","t"}, PropagatorType->Straight,
PropagatorArrow->Forward},
 F[9] == { ClassName->dq, SelfConjugate->False, Indices-
>{Index[GEN],Index[Colour]}, FlavorIndex->GEN, QuantumNumbers->{Q->-1/3},
WeylComponents->{dLw,DRwbar},
      ParticleName->{"d","s","b"}, AntiParticleName->{"d~","s~","b~"},
ClassMembers->{d,s,b},
      Mass->{Mdq,{MD,5.04*^-3}, {MS,0.101}, {MB,4.7}}, Width->0, PDG->{1,3,5},
      PropagatorLabel->{"dq","d","s","b"}, PropagatorType->Straight,
```

```
PropagatorArrow->Forward}
};

(* ************************* *)
(* *****   Parameters   ***** *)
(* ************************* *)
M$Parameters = {

(* Electroweak and QCD inputs *)
 aEWM1 == { TeX->Subsuperscript[\[Alpha],w,-1], ParameterType->External,
BlockName->SMINPUTS, OrderBlock->1, Value->127.9,       InteractionOrder->{QED,-
2},
    Description->"Inverse of the EW coupling constant at the Z pole"},
 Gf    == { TeX -> Subscript[G,f],              ParameterType->External,
BlockName->SMINPUTS, OrderBlock->2, Value->1.16637*^-5, InteractionOrder->{QED,
2},
    Description->"Fermi constant"},
 aS    == { TeX->Subscript[\[Alpha],s],         ParameterType->External,
BlockName->SMINPUTS, OrderBlock->5, Value->0.1184, InteractionOrder->{QCD, 2},
    Description->"Strong coupling constant at the Z pole."},
 aEW == { TeX->Subscript[\[Alpha],EW], ParameterType->Internal, Value-> 1/aEWM1,
InteractionOrder->{QED,2},
    Description -> "Electroweak coupling constant" },
 cabi == { TeX -> Subscript[\[Theta], c], ParameterType -> External, BlockName
-> CKMBLOCK, OrderBlock -> 1,Value -> 0.227736, Description -> "Cabibbo
angle" },

(* New Physics (NP) inputs *)
 cphi == { TeX -> Subscript[c,\[Phi]], ParameterType -> External, BlockName-
>NPINPUTS, OrderBlock->1, Value ->0.2,
    Description -> "Cosine of the U(1)X / SU(2)_2 mixing angle"},
 xx  == { TeX -> x, ParameterType -> External, BlockName->NPINPUTS, OrderBlock-
>2, Value ->200.,
    Description -> "Ratio of the two symmetry breaking scales"},
 s2b == { TeX -> Subscript[t,\[Beta]], ParameterType -> External, BlockName-
>NPINPUTS, OrderBlock->3, Value ->0.25,
    Description -> "Sine of twice the Higgs beta angle"},
 TripletFlag == {  ParameterType -> External, BlockName->NPINPUTS, OrderBlock-
>4, Value ->1},


(* Weak mixing angles *)
 c2b == { ParameterType -> Internal, Value -> Sqrt[1-s2b^2],
    Description-> "Cosine of twice the Higgs beta angle" },
 sb == { TeX->Subscript[s,\[Beta]], ParameterType->Internal, Value->Sqrt[1/2(1-
c2b)],
    Description->"Sine of the beta angle"},
 sphi == { TeX->Subscript[s,\[Phi]], ParameterType->Internal, Value->Sqrt[1-
cphi^2],
    Description->"Sine of the U(1)X / SU(2)_2 mixing angle"},
 s2th== { ParameterType -> Internal, Value -> Sqrt[4*Pi aEW/(Sqrt[2] MZ^2 Gf)
(1-1/xx(cphi^4/(1+3*TripletFlag)-s2b^2/(1+TripletFlag)))],
    Description-> "Sine of twice the U(1)Y / SU(2)_L mixing angle" },
 c2th== { ParameterType -> Internal, Value -> Sqrt[1-s2th^2],
    Description-> "Cosine of twice the U(1)Y / SU(2)_L mixing angle" },
 sth == { TeX->Subscript[s,\[Theta]], ParameterType->Internal, Value-
>Sqrt[1/2(1-c2th)],
    Description->"Sine of the U(1)Y / SU(2)_L mixing angle"},
 cth == { TeX->Subscript[c,\[Theta]], ParameterType->Internal, Value-
>Sqrt[1/2(1+c2th)],
    Description->"Cosine of the U(1)Y / SU(2)_L mixing angle"},

(* coupling constants *)
 ee == { TeX -> e, ParameterType -> Internal, Value -> Sqrt[4 Pi aEW],
```

```
InteractionOrder -> {QED,1},
    Description -> "Electromagnetic coupling constant"},
 g1 == { TeX->Subscript[g,1], ParameterType->Internal, Definitions->{g1-
>ee/sth}, InteractionOrder->{QED,1},
   Description->"SU(2)_1 coupling constant"},
 g2 == { TeX->Subscript[g,2], ParameterType->Internal, Definitions->{g2->ee/
(sphi cth)}, InteractionOrder->{QED,1},
   Description->"SU(2)_2 coupling constant"},
 gX == { TeX->Subscript[g,X], ParameterType->Internal, Definitions->{gX->ee/
(cphi cth)}, InteractionOrder->{QED,1},
   Description->"U(1)X coupling constant"},
 gs == { TeX -> Subscript[g,s], ParameterType -> Internal, Value -> Sqrt[4 Pi
aS], InteractionOrder -> {QCD,1},
   ParameterName -> G, Description -> "Strong coupling constant at the Z
pole" },

(* Masses *)
 vev == { ParameterType -> Internal, Value -> Sqrt[1/Sqrt[2]/Gf*(1+s2b^2/
((1+TripletFlag)*xx))],  InteractionOrder -> {QED,-1},
    Description-> "Higgs vacuum expectation value" },
 MW == { TeX -> Subscript[M,W], ParameterType -> Internal,  Value -> ee vev/(2
sth) (1-sb^2/(2 (1+TripletFlag) xx)),
    Description -> "W mass" },
 MZp == { TeX -> Subscript[M,Z'], ParameterType -> Internal,  Value ->
Sqrt[1/4*(g2^2+gX^2)*xx*vev^2*(1+3*TripletFlag) + cphi^2/4*g2^2*vev^2],
    Description -> "Zp mass" },
 MWp == { TeX -> Subscript[M,W'], ParameterType -> Internal,  Value ->
Sqrt[1/4*g2^2*xx*vev^2*(1+TripletFlag) + 1/4 g2^2*vev^2],
    Description -> "Wp mass" },

 (* CKM matrices *)
 CKM == {  TeX -> Superscript[V,CKM], ParameterType -> Internal, Indices ->
{Index[GEN], Index[GEN]}, Unitary -> True,
   Value -> {CKM[1,1] -> Cos[cabi], CKM[1,2] -> Sin[cabi], CKM[1,3] -> 0,
CKM[2,1] -> -Sin[cabi], CKM[2,2] -> Cos[cabi], CKM[2,3] -> 0, CKM[3,1] -> 0,
CKM[3,2] -> 0, CKM[3,3] -> 1},
   Description -> "CKM-Matrix"}

};

(* ************************* *)
(* *****   Lagrangian   ***** *)
(* ************************* *)

LGauge := -1/4ExpandIndices[FS[BX,mu,nu] FS[BX,mu,nu] + FS[W1i,mu,nu,ii]
FS[W1i,mu,nu,ii] + FS[W2i,mu,nu,ii] FS[W2i,mu,nu,ii] + FS[G,mu,nu,aa]
FS[G,mu,nu,aa]];

LFermions := Block[{LLag},
  LLag = ExpandIndices[
    -I QLwbar[sp1, i1, fl, cc].DC[QLw[sp2, i1, fl, cc], mu] sibar[mu, sp1, sp2]
-
     I QRwbar[sp1, i1, fl, cc].DC[QRw[sp2, i1, fl, cc], mu] sibar[mu, sp1, sp2]
-
     I LLwbar[sp1, i1, fl].DC[LLw[sp2, i1, fl], mu] sibar[mu, sp1, sp2] -
     I LRwbar[sp1, i1, fl].DC[LRw[sp2, i1, fl], mu] sibar[mu, sp1, sp2],
      FlavorIndex -> {SU2W1, SU2W2, SU2D1, SU2D2}];
  Colourb=Colour;
  LLag=LLag/.Tb[a_,i_,j_]->-T[a,j,i];
  Return[WeylToDirac[LLag]];
];

LWPLR:= LGauge + LFermions;
```